Available online at www.sciencedirect.com
ScienceDirect
Remote Sensing of Environment 112 (2008) 901–919
Remote Sensing of Environment
www.elsevier.com/locate/rse

Global estimates of the land–atmosphere water flux based on monthly AVHRR and ISLSCP-II data, validated at 16 FLUXNET sites

Joshua B. Fisher [a,*], Kevin P. Tu [b], Dennis D. Baldocchi [a]

[a] Department of Environmental Science, Policy and Management, University of California at Berkeley, USA
[b] Department of Integrative Biology, University of California at Berkeley, USA

Received 1 December 2005; received in revised form 12 June 2007; accepted 30 June 2007

Abstract

Numerous models of evapotranspiration have been published that range in data-driven complexity, but global estimates require a model that does not depend on intensive field measurements. The Priestley–Taylor model is relatively simple, and has proven to be remarkably accurate and theoretically robust for estimates of potential evapotranspiration. Building on recent advances in ecophysiological theory that allow detection of multiple stresses on plant function using biophysical remote sensing metrics, we developed a bio-meteorological approach for translating Priestley–Taylor estimates of potential evapotranspiration into rates of actual evapotranspiration. Five model inputs are required: net radiation (R_n), normalized difference vegetation index (NDVI), soil adjusted vegetation index (SAVI), maximum air temperature (T_{max}), and water vapor pressure (ea). Our model requires no calibration, tuning or spin-ups. The model is tested and validated against eddy covariance measurements (FLUXNET) from a wide range of climates and plant functional types—grassland, crop, and deciduous broadleaf, evergreen broadleaf, and evergreen needleleaf forests. The model-to-measurement r^2 was 0.90 (RMS = 16 mm/month or 28%) for all 16 FLUXNET sites across 2 years (most recent data release). Global estimates of evapotranspiration at a temporal resolution of monthly and a spatial resolution of 1° during the years 1986–1993 were determined using globally consistent datasets from the International Satellite Land-Surface Climatology Project, Initiative II (ISLSCP-II) and the Advanced Very High Resolution Spectroradiometer (AVHRR). Our model resulted in improved prediction of evapotranspiration across water-limited sites, and showed spatial and temporal differences in evapotranspiration globally, regionally and latitudinally.

Keywords: Evapotranspiration; Water flux; FLUXNET; AmeriFlux; Eddy flux; MODIS; International Land-Surface Climatology Project; ISLSCP; ISLSCP-II; Remote sensing; Model; Ecophysiology; Priestly–Taylor; Global

1. Introduction

Evapotranspiration (LE) is a major component in the processes and models of global climate change, water balance, net primary productivity, floods, droughts, and irrigation. LE is difficult to measure and predict, however, especially at large spatial scales (Turner, 1989). Understanding the variability in water cycle processes requires a spatially detailed analysis of global land surface processes (Running et al., 2000). Closing the water budget worldwide is of utmost importance to water and energy cycle research; the overall goal of which is to deliver reliable estimates of precipitation and LE over the whole surface of the earth using a combination of measurements and model estimates (Entekhabi et al., 1999).

Global LE estimation in the literature has been marked by a struggle between realistic models that are hindered by complex parameterization and simple models that lack mechanistic realism (Cleugh et al., 2007). The trend has been towards increasing complexity, as opposed to applicability (Federer et al., 1996). Yet, greater complexity requires detailed input parameters that limit application to areas where the necessary data are available (Federer et al., 2003; Kustas & Norman, 1996). Before the widespread ecological application of remote sensing data, researchers estimated regional LE with interpolated data from thousands of meteorological stations (Baumgartner & Reichel, 1975; Budyko, 1978; Hare, 1980; Morton, 1983).

* Corresponding author.
E-mail address: joshbfisher@gmail.com (J.B. Fisher).

0034-4257/$ - see front matter © 2007 Elsevier Inc. All rights reserved.
doi:10.1016/j.rse.2007.06.025

Table 1
Model parameters and equations. R_n is net radiation, R_{nc} is net radiation to the canopy ($R_n - R_{ns}$), R_{ns} is net radiation to the soil ($R_n \exp(-k_{Rn}\mathrm{LAI})$) (Beer, 1852; Bouguer, 1729; Denmead, 1976; Lambert, 1760), LAI is total (green+non-green) leaf area index ($-\ln(1-f_c)/k_{PAR}$) (Ross, 1976), G is ground heat flux, T_{max} is maximum air temperature, RH is relative humidity, VPD is saturation vapor pressure deficit, Δ is slope of saturation-to-vapor pressure curve, γ is the psychrometric constant (~0.066 kPa $°C^{-1}$). α=1.26 (Priestley & Taylor 1972), β=1.0 kPa, k_{Rn}=0.6 (Impens & Lemur, 1969), k_{PAR}=0.5 (Ross, 1976), m_1=1.2*1.136, b_1=1.2*−0.04 (Gao et al., 2000; Huete, 2006; Huete, 1988), m_2=1.0, b_2=−0.05 (This study; assumes 0.05<NDVI<1.0 and 0<f_{IPAR}<0.95), $\lambda = T_{opt}$ (This study)

Parameter	Description	Equation	Reference
LE	Evapotranspiration	$LE_s + LE_c + LE_I$	
LE_c	Canopy transpiration	$(1 - f_{wet}) f_g f_T f_M \alpha \frac{\Delta}{\Delta+\gamma} R_{nc}$	This study; Priestley and Taylor (1972)
LE_s	Soil evaporation	$(f_{wet} + f_{SM}(1-f_{wet}))\alpha \frac{\Delta}{\Delta+\gamma}(R_{ns} - G)$	This study; Priestley and Taylor (1972)
LE_i	Interception evaporation	$f_{wet} \alpha \frac{\Delta}{\Delta+\gamma} R_{nc}$	This study; Priestley and Taylor (1972)
f_{wet}	Relative surface wetness	RH^4	This study
f_g	Green canopy fraction	$\frac{f_{APAR}}{f_{IPAR}}$	
f_T	Plant temperature constraint	$\exp\left(-\left(\frac{T_{max}-T_{opt}}{\lambda}\right)^2\right)$	June et al. (2004)
f_M	Plant moisture constraint	$\frac{f_{APAR}}{f_{APARmax}}$	This study
f_{SM}	Soil moisture constraint	$RH^{VPD/\beta}$	This study
f_{APAR}	Fraction of PAR absorbed by green vegetation cover	$m_1 SAVI + b_1$	Gao et al. (2000), Huete (2006)
f_{IPAR}	Fraction of PAR intercepted by total vegetation cover	$m_2 NDVI + b_2$	This study
f_c	Fractional total vegetation cover	f_{IPAR}	Campbell and Norman (1998)
T_{opt}	Optimum plant growth temperature	T_{max} at max{PAR$f_{APAR}T_{max}$/VPD}	This study

LE methods – Thornthwaite (1948), Priestley and Taylor (1972), and Monteith (1965) – continue to be used with different theoretical (and subsequent operational) modifications to generate global patterns of LE (Choudhury, 1997; Choudhury & DiGirolamo, 1998; Choudhury et al., 1998; Cleugh et al., 2007; Gordon et al., 2005; Houborg & Soegaard, 2004; Mintz & Walker, 1993; Nishida et al., 2003; Tateishi & Ahn, 1996). The Penman–Monteith equation is more theoretically accurate than are the Priestley–Taylor or Thornthwaite methods, but requires parameters that are difficult to characterize globally such as aerodynamic resistance, stomatal resistance, and wind speed. Still, the Penman–Monteith and Priestley–Taylor methods have been shown to give relatively low biases, particularly in comparison with the relatively poor accuracy of the Thornthwaite method (Vörösmarty et al., 1998). The potential LE equations, however, must be reduced to actual LE based on soil moisture (Federer et al., 2003; Maurer et al., 2002). Further constraints by temperature and soil-canopy partitioning may be implemented (McNaughton & Spriggs, 1986).

Two major datasets are being used to drive and validate global LE estimates. A global network of eddy covariance towers – FLUXNET – provides measurements of water and energy fluxes over 0.5–5 km^2 across a wide range of ecosystems and climates (Baldocchi et al., 2001). Nishida et al. (2003) validated their NOAA/AVHRR-driven model of evaporative fraction across 13 sites in the AmeriFlux network (r^2=0.71). Houborg and Soegaard (2004) validated their MODIS/AVHRR-driven model with flux measurements in Denmark (r^2=0.58–0.85). Both Nishida et al. and Houborg and Soegaard based their LE models on modified Penman–Monteith approaches. The second major dataset – the International Satellite Land Surface Climatology Project Initiative II (ISLSCP-II) – is one of several projects within the Global Hydrology Project of the Global Energy and Water Cycle Experiment (GEWEX), and is a compilation of data sources from a suite of satellites and aggregation of complementary and supplementary ground measurements (Los et al., 2000). ISLSCP-II spans a decade and supports investigations of the global carbon, water and energy cycle. Lawrence and Slingo (2004) used ISLSCP-II to assess the impact on evaporation by vegetation within a general circulation model.

We combine FLUXNET, ISLSCP-II, AVHRR and the Priestley and Taylor (1972) method here with new ecophysiological ideas on how to reduce potential to actual LE when soil moisture, stomatal resistance and wind speed data are unavailable, which is the case for most parts of the globe (De Bruin & Stricker, 2000). Furthermore, recent estimates of LE using aerodynamic resistance–surface energy balance models have failed (Cleugh et al., 2007). Our model instead relies on four plant physiological limitations to LE and one soil drought constraint as proxies to these variables. Our ultimate aim is to evaluate actual LE at the global scale.

Although the Priestley–Taylor method works very well as a potential LE model across most surface conditions under its original form and at α=1.26 (Eichinger et al., 1996), numerous attempts at adjusting the Priestley–Taylor coefficient have been made to connect potential to actual LE (Baldocchi & Meyers, 1998; Barton, 1979; Black, 1979; Davies & Allen, 1973; De

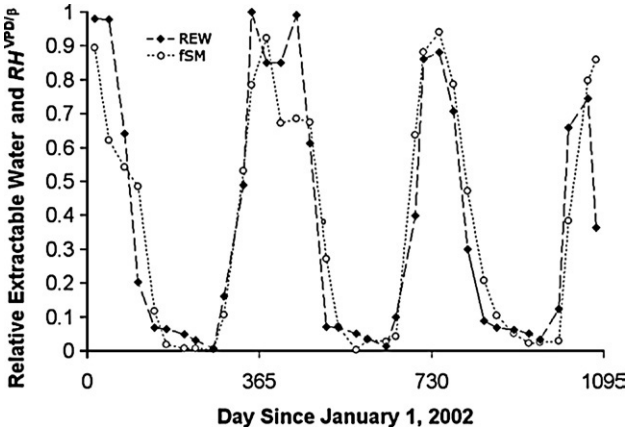

Fig. 1. Comparison of monthly f_{SM} to normalized volumetric water content (VWC), or relative extractable water – REW=(VWC−VWC_{min})/(VWC_{max}−VWC_{min}) – at an oak–savanna site.

Table 2
AmeriFlux sites used for model validation. Additional site information can be found at http://public.ornl.gov/ameriflux/

Site	Biome type	Latitude	Longitude	P.I.
Bondville	Temperate C3/C4 crop	40° 0′ 21.96″ N	88° 17′ 30.72″ W	T. Myers
Griffin	Temperate evergreen needleleaf forest	56° 36′ 23.59″ N	3° 47′ 48.55″ W	J. Moncrieff
Hainich	Temperate deciduous broadleaf forest	51° 4′ 45.36″ N	10° 27′ 7.2″ E	A. Knohl
Hesse	Temperate deciduous broadleaf forest	48° 40′ 27″ N	7° 3′ 56″ E	A. Granier
Howland	Cold-temperate evergreen needleleaf forest	45° 12′ 14.65″ N	68° 44′ 25″ W	D. Hollinger
Mer Bleue	Boreal wetland	45° 24′ 33.84″ N	75° 31′ 12″ W	P. Lafleur
Mize	Subtropical evergreen needleleaf forest	29° 45′ 53.28″ N	82° 14′ 41.34″ W	T. Martin
Morgan Monroe	Temperate deciduous broadleaf forest	39° 19′ 23.34″ N	86° 24′ 47.30″ W	H. Schmid
Niwot	Sub-alpine evergreen needleleaf forest	40° 01′ 57″ N	105° 32′ 49″ W	R. Monson
NSA-OBS	Boreal evergreen needleleaf forest	55° 52′ 46.63″ N	98° 28′ 50.91″ W	S. Wofsy
Takayama	Cold-temperate deciduous broadleaf forest	36° 08′ 46.2 N	137° 25′ 23.2″ E	S. Yamamoto
Tapajos (67 m)	Tropical evergreen broadleaf forest	2° 51′ 24″ S	54° 57′ 32″ W	S. Wofsy
Tonzi	Mediterranean savanna	38° 25′ 53.76″ N	120° 57′ 57.54″ W	D. Baldocchi
Tumbarumba	Temperate evergreen broadleaf forest	35° 39′ 20.6″ S	148° 9′ 7.5″ E	R. Leuning
Virginia Park	Woody savanna	19° 52′ 59″ S	146° 33′ 14″ E	R. Leuning
Walnut River	Temperate C3/C4 grassland	37° 31′ 15″ N	96° 51′ 18″ W	R. Coulter

Bruin & Holtslag, 1982; Fisher et al., 2005; Flint & Childs, 1991; Giles et al., 1984; Jury & Tanner, 1975; McNaughton & Black, 1973; Mukammal & Neumann, 1977; Shuttleworth & Calder, 1979; Stewart & Rouse, 1977). We keep α constant at 1.26 so that the Priestley–Taylor equation as a potential LE equation remains intact as originally designed and confirmed. Subsequently, the novelty in our approach is to scale-down potential LE to actual LE based on ecophysiological constraints and soil evaporation partitioning.

Our model requires no site calibration, tuning or spin-ups, and is applied on a per-pixel basis. We validate our model "on the ground" with eddy covariance data from 16 FLUXNET sites. These sites range from tropical to boreal environments and represent a wide range of plant functional types—grassland, crop, and deciduous broadleaf, evergreen broadleaf, and evergreen needleleaf forests. Next, we provide new global estimates of the land–atmosphere water flux as driven by ISLSCP-II global datasets.

2. Methods

2.1. Model description

Our model of LE is partitioned into canopy transpiration (LE_c), soil evaporation (LE_s), and interception evaporation (LE_i). Total evapotranspiration, LE, is calculated as the sum of $LE_c+LE_s+LE_i$. The Priestley and Taylor (1972) equation for potential LE based on available energy is used for each component flux, and each is controlled by ecophysiological constraints or conditions to reduce potential LE to actual LE based on plant physiological status and soil moisture availability (Table 1). The model is driven with five inputs: net radiation (R_n), normalized difference vegetation index (NDVI), soil adjusted vegetation index (SAVI), maximum air temperature (T_{max}), and water vapor pressure (ea). Soil heat flux (G) should be included in available soil energy ($R_{ns}-G$), but where G is unavailable R_{ns} may be used alone (Kustas et al., 1993); G is assumed to be close to zero at monthly time steps, but can be calculated from spectral indices (Choudhury et al., 1987; Clothier et al., 1986; Daughtry et al., 1990; Kustas & Daughtry, 1990). NDVI is calculated as $(r_{NIR}-r_{VIS})/(r_{NIR}+r_{VIS})$, and SAVI is calculated as $(1.5)(r_{NIR}-r_{VIS})/(r_{NIR}+r_{VIS}+0.5)$ (Huete, 1988).

We calculate four plant physiological limitations to LE_c: 1) leaf area index (LAI), 2) green fraction of the canopy that is actively transpiring (f_g), 3) plant temperature constraint (f_T), and 4) plant moisture constraint (f_M). LAI is an indication of the biophysical capacity for energy acquisition by the canopy and f_g reflects the biophysical capacity for energy absorptance by the functional green leaf area fraction. We hypothesize that plants optimize investment in energy acquisition such that this biophysical capacity changes in parallel with the physiological capacity for transpiration. Further, either total LAI or f_g decreases (either or both, depending on the particular plant strategy) in response to soil drought and chronic stomatal closure resulting from prolonged atmospheric drought (high vapor pressure deficit). LAI was calculated from total fractional vegetation cover (f_c) by inverting Beer's law (e.g., Norman et al., 1995). f_c was assumed equal to light intercepted by the vegetated fraction of the land surface (f_{IPAR}).

f_g was calculated as the ratio of light absorptance by the green fraction of the land surface (f_{APAR}) to f_{IPAR}. f_{IPAR} was estimated as a linear function of NDVI (Zhang et al., 2005), whereas f_{APAR} should be estimated as a linear function of the Enhanced Vegetation Index (EVI) (Gao et al., 2000; Xiao et al., 2003; Zhang et al., 2005). SAVI was used instead of EVI because the latter requires blue reflectance information from the land surface and is not available from the AVHRR sensor. However, SAVI and EVI are functionally very similar, with SAVI only lacking the often small atmospheric corrections included in EVI (Huete et al., 2002). Both SAVI and EVI provide soil corrections that lead to a more accurate and robust indication of green vegetation cover relative to NDVI (Gao et al., 2000).

The plant temperature constraint, f_T follows the equation detailed by June et al. (2004) with an optimum T_{max} (T_{opt}) calculated following the Potter et al. (1993) CASA model as the T_{max} at the time of peak canopy activity. We updated this

Fig. 2. The 16 FLUXNET sites used in the validation spanned across N. America, S. America, Europe, Asia, and Australia.

approach by considering not only light absorptance as an indication of canopy activity, but also the seasonality of air temperature and vapor pressure deficit (VPD). We assume that when leaves are present, the optimal canopy stomatal conductance occurs when green leaf area, light, and temperature are high and VPD is low.

The plant moisture constraint, f_M was estimated from the relative change in light absorptance ($f_{APAR}/f_{APARmax}$) assuming that light absorptance primarily varies in response to moisture stress (Potter et al., 1993). We further assume that no moisture stress occurs before peak light absorptance, when the canopy is actively growing and water stress should be minimal. At moist sites f_M plays only a minor role—its contribution is primarily limited to sites that experience seasonal drought.

We constrain LE_s by f_{SM}, which is an index of soil water deficit based on the complementary hypothesis of Bouchet (1963) whereby surface moisture status is linked to and reflects the evaporative demand of the atmosphere. The assumption is that soil moisture is reflected in the adjacent atmospheric moisture. This link is compromised, however, by including periods when humidity changes independently of soil moisture such as at night when relative humidity (RH) will tend towards 100% due to cooling temperatures. The strongest link therefore between atmospheric and soil moisture is midday during convective conditions with strong vertical mixing and influence of surface conditions on the atmosphere. Thus, we use midday conditions (i.e., RH_{min}, T_{max}) rather than daily averages for this calculation. Another problem exists, however, when the vertically adjacent atmosphere is not in equilibrium with the underlying soil. This is the case of advection when humid air comes in to a system with dry soil from a laterally adjacent moist source. Over large enough spatial and temporal scales, however, the surface tends to be in equilibrium with the overlying atmosphere and f_{SM} is a good indication of soil moisture. Recognizing that evaporation is intrinsically driven by VPD, we seek a relative index such as RH that is sensitive to VPD. Using RH alone assumes a linear relationship with f_{SM}. Initial inspection indicates lower than expected f_{SM} at high VPD, however, and higher than expected f_{SM} at low VPD. We therefore parameterize f_{SM} as $RH^{VPD/\beta}$, with β defining the relative sensitivity to VPD. RH and VPD were calculated from the vapor pressure (ea) and the saturation vapor pressure of the air (es), the latter based on T_{max}. In practice, if data are available for RH and VPD, then ea is not needed. Because f_{SM} is an index scaled between 0 and 1, we must scale soil moisture, or soil volumetric water (VWC, $m^3 \cdot m^{-3}$), between 0 and 1 for comparison and validation. We therefore define relative extractable water (REW) as: $REW = (VWC - VWC_{min})/(VWC_{max} - VWC_{min})$. f_{SM} follows REW closely (Fig. 1); VWC was measured with time domain reflectometry at the Tonzi flux site.

LE_i, which is the evaporation of canopy-intercepted precipitation, is calculated as potential LE multiplied by the fraction of time when the surface that is wet (f_{wet}). The latter was scaled to relative humidity (RH) using a power function to reflect the time scale on which it changes ($f_{wet} = RH^4$). This function effectively predicts 0% wet surfaces at RH < 70%, 50% at RH = 93%, and 100% at RH = 100%. This type of approach has been used in global modeling efforts (Stone et al., 1977) and provides a reasonable representation of surface wetness as compared to CRU estimates based on observed precipitation (monthly $r^2 \sim 0.60$, data not shown). Stone et al. used an empirical function of surface RH to estimate ground wetness in the GISS general circulation model.

2.2. Data: validation sites

We validated the model across a wide range of ecosystems, climates and functional types at 16 FLUXNET sites for 2000–2003 (Table 2 and Fig. 2) (Flanagan et al., 2002; Goldstein et al., 2000; Granier et al., 2000; Hollinger et al., 1999; Knohl et al., 2003; Leuning et al., 2005; Martin et al., 1997; Moncrieff et al., 1997; Monson et al., 2002; Schmid et al., 2000; Xu & Baldocchi, 2004). These sites represent 6 sub-networks of FLUXNET: AmeriFlux, AsiaFlux, CarboEuroFlux, Fluxnet-Canada, LBA, and OzFlux. For the validation part of this analysis, we used in situ measurements of R_n, T_{max} and ea obtained from each study site to test the accuracy of the model (rather than using remote sensing meteorological data to test the accuracy of the input variables). The model predictions presented here were calculated using monthly[1] means of these measurements. NDVI and SAVI for the sites were determined from the Moderate Resolution Imaging Spectroradiometer (MODIS). The Oak Ridge National Laboratory Distributed Active Archive Center (ORNL DAAC) subsets the full MODIS scenes (1200-km × 1200-km) to 7-km × 7-km areas containing the flux towers.

Our predicted LE was compared against the LE measured by the eddy covariance method (Baldocchi et al., 1988) at the towers for the respective range of footprints (roughly 0.5–5 km^2). The eddy covariance method quantifies vertical fluxes of scalars between the ecosystem and the atmosphere from the covariance between vertical wind velocity and scalar fluctuations at 10 Hz, and we compute monthly averages to coincide with the global monthly outputs (e.g., Baldocchi et al., 1988; Shuttleworth et al., 1984; Wofsy et al., 1993). We did not gap fill eddy covariance data because our aim was not to report total

[1] At shorter time steps, the model requires 8-day means of midday R_n, T_{max} and ea as well as instantaneous R_n and T_{max}.

Table 3
Datasets used for flux site validation and global estimation

Parameter	Description	Source
FLUXNET validation		
R_n	Net radiation	FLUXNET
T_{max}	Air temperature	FLUXNET
RH	Relative humidity	FLUXNET
VPD	Vapor pressure deficit	FLUXNET
r_{vis}	Visible spectrum reflectance	MODIS
r_{NIR}	Near-infrared spectrum reflectance	MODIS
Global estimates		
R_n	Net radiation	ISLSCP-II
T_{max}	Air temperature	ISLSCP-II
ea	Water vapor pressure	ISLSCP-II
r_{vis}	Visible spectrum reflectance	AVHRR
r_{NIR}	Near-infrared spectrum reflectance	AVHRR

Table 4
Predicted to measured LE r^2's for each flux site

Site	Biome type	r^2
Bondville	Temperate C3/C4 crop	0.91
Griffin	Temperate evergreen needleleaf forest	0.92
Hainich	Temperate deciduous broadleaf forest	0.94
Hesse	Temperate deciduous broadleaf forest	0.93
Howland	Cold-temperate evergreen needleleaf forest	0.86
Mer Bleue	Boreal wetland	0.96
Mize	Subtropical evergreen needleleaf forest	0.89
Morgan Monroe	Temperate deciduous broadleaf forest	0.96
Niwot	Sub-alpine evergreen needleleaf forest	0.88
NSA-OBS	Boreal evergreen needleleaf forest	0.82
Takayama	Cold-temperate deciduous broadleaf forest	0.78
Tapajos (67 m)	Tropical evergreen broadleaf forest	0.55
Tonzi	Mediterranean savanna	0.83
Tumbarumba	Temperate evergreen broadleaf forest	0.89
Virginia Park	Woody savanna	0.81
Walnut River	Temperate C3/C4 grassland	0.96

fluxes, but to test the model predictions for the times when valid data were available. Our validation was limited to these sites due to data use permission, applicable measurements, and/or available recent measurements (to correspond to recent satellite remote sensing measurements).

Our model predicts LE as the sum of LE_c, LE_s and LE_i. Because direct measurements of these component fluxes are rare, we tested LE_c and LE_s (LE_i relatively minimal) predictions against indirect estimates determined using a physically-based energy balance partitioning method. This method was similar to that of Massman (1992), which was validated using sap flow measurements of transpiration by Massman and Ham (1994). We validated the method at three tower flux sites that measured surface radiative temperature (modified from soil surface radiative temperature) as required by the method. The sites represent a range of plant functional types and climatic conditions: Morgan Monroe (temperature deciduous forest), Niwot Ridge (sub-alpine evergreen needleleaf forest), and Bondville (temperate C_3/C_4 crop). In this modified approach, LE is partitioned using the two-source soil and canopy model of Shuttleworth and Wallace (1985).

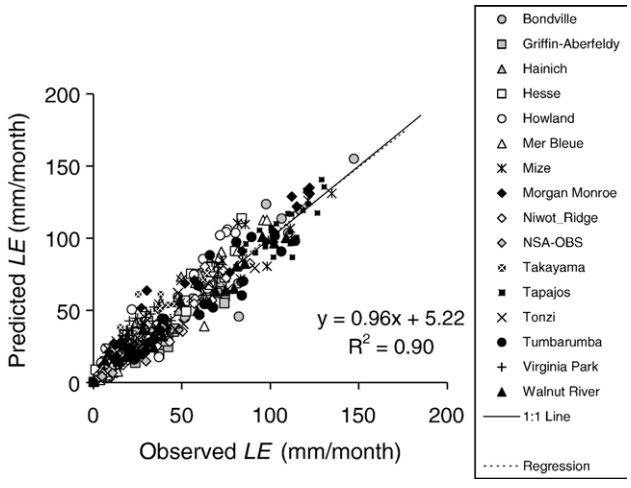

Fig. 3. Testing the model against tower measurements of LE. Shown are monthly sums of LE (mm/month) for 2 years at each of sixteen tower flux sites from around the world.

2.3. Data: global estimates

For global estimates of LE, we used input datasets for R_n, T_{max} and ea from the ISLSCP-II archive for 1986–1993 (Hall et al., 2005; Los et al., 2000; Sellers et al., 1995). ISLSCP-II data are 1° gridded monthly values, which are appropriate for LE estimation at the global scale (Federer et al., 1996). ISLCP-II used Surface Radiation Budget (SRB) data for R_n (Stackhouse et al., 2000), based on meteorological inputs taken from Goddard Earth Observing System version 1 (GEOS-1) reanalysis data sets (Schubert et al., 1993) by the Data Assimilation Office at NASA Goddard Space Flight Center. Cloud parameters and surface albedos were derived from the International Satellite Cloud Climatology Project data (Pinker & Laszlo, 1992; Rossow et al., 1996). Random errors in monthly average shortwave and longwave fluxes are between 10–15 $W \cdot m^{-2}$ (Stackhouse et al., 2000). ISLSCP-II provided Fourier-adjusted, sensor and solar zenith angle corrected, interpolated, reconstructed (FASIR) adjusted NDVI (Los et al., 2000). ISLSCP-II T_{max} and ea were from the Climate Research Unit Monthly Climate Data (New et al., 1999; New et al., 2000). These data were interpolated directly from station observations, merged datasets, and from synthetic data estimated using predictive relationships with precipitation and temperature measurements. ISLSCP-II was unable to quantify the errors in T_{max} and ea, but we report in the Discussion related research on these errors. T_{max} was calculated from ISLSCP-II mean and diurnal air temperature.

Because ISLSCP-II did not provide SAVI, and because MODIS could not provide the temporal history to match with ISLSCP-II, we calculated SAVI from 1° AVHRR data. We adjusted AVHRR SAVI to be consistent with the FASIR adjusted NDVI by multiplying by the ratio of FASIR NDVI to

AVHRR NDVI. We assume as a first approximation that correction factors for sensor degradation, aerosol effects, cloud contamination, solar zenith angle variations, and missing data apply equally to NDVI and SAVI. Visible and near-infrared reflectances were obtained from the NOAA/NASA Pathfinder AVHRR dataset (http://disc.sci.gsfc.nasa.gov/landbio/). AVHRR channel 1 (r_{VIS}) records wavelengths from 0.58–0.68 μm; channel 2 (r_{NIR}) records wavelengths from 0.73–1.10 μm. The theoretical range of SAVI and NDVI is between −1 and 1, but the actual measured range from the satellite data ranged from 0 to 0.9 for both indices. We follow Steven et al. (2003) for sensor calibration. A more detailed, comprehensive description of the NOAA series satellites, the AVHRR instrument and data can be found in the NOAA Polar Orbiter Data User's Guide (Kidwell, 1991).

Data were processed in MATLAB 6.5, ESRI's ArcGIS 9.1, ImageJ (http://rsb.info.nih.gov/ij/), and Microsoft Excel. AmeriFlux/FLUXNET data can be downloaded at http://daac.ornl.gov/FLUXNET/. ISLSCP-II data can be downloaded at http://islscp2.sesda.com/ISLSCP2_1/html_pages/islscp2_home.html. The datasets used for the site validation and global estimates are separate, but comparable (Table 3).

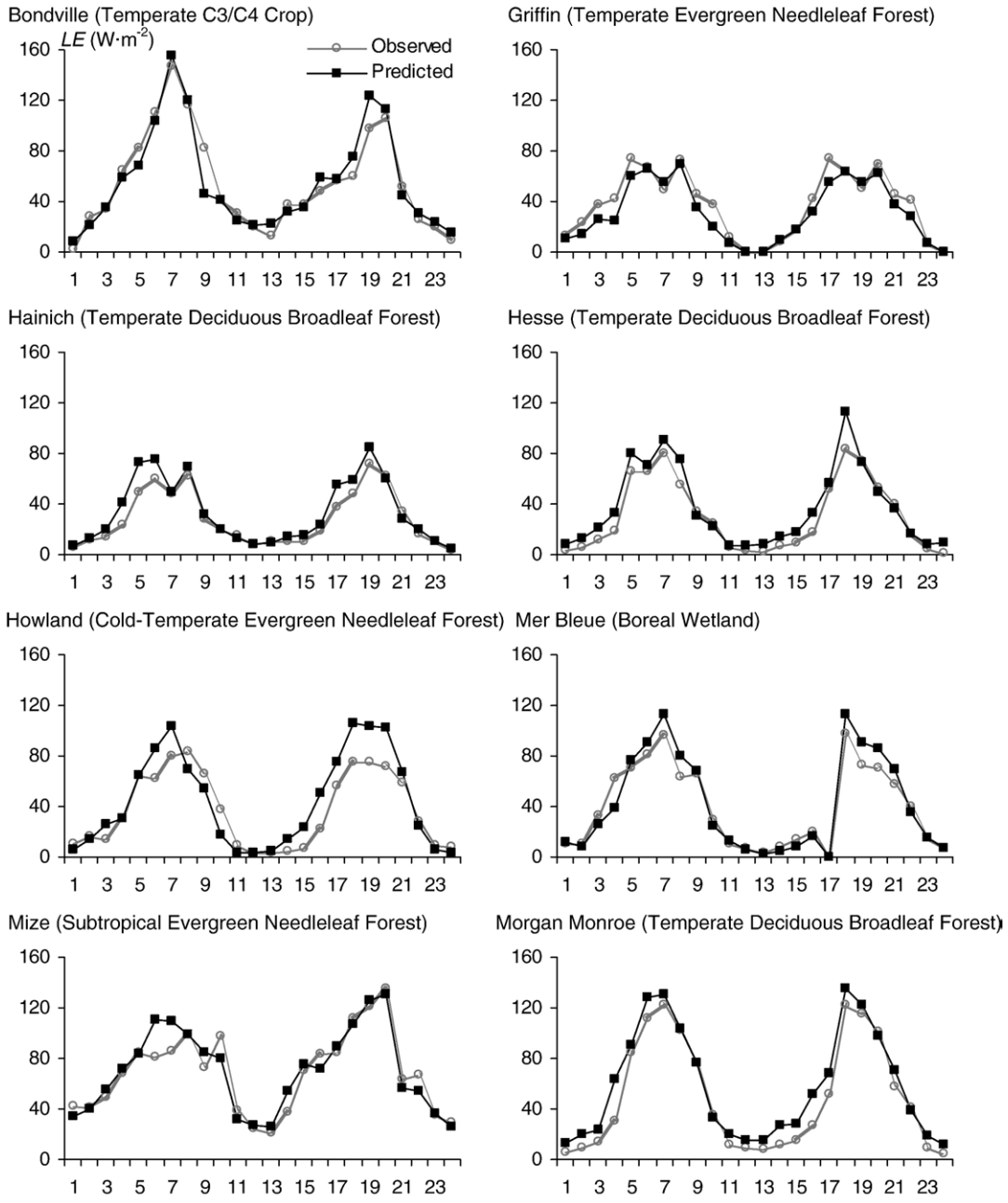

Fig. 4. Two-year monthly time series by of tower measurements and model predictions at each site. *y*-axis is LE ($W \cdot m^{-2}$) and *x*-axis is month. Closed squares are predicted and open circles are observed.

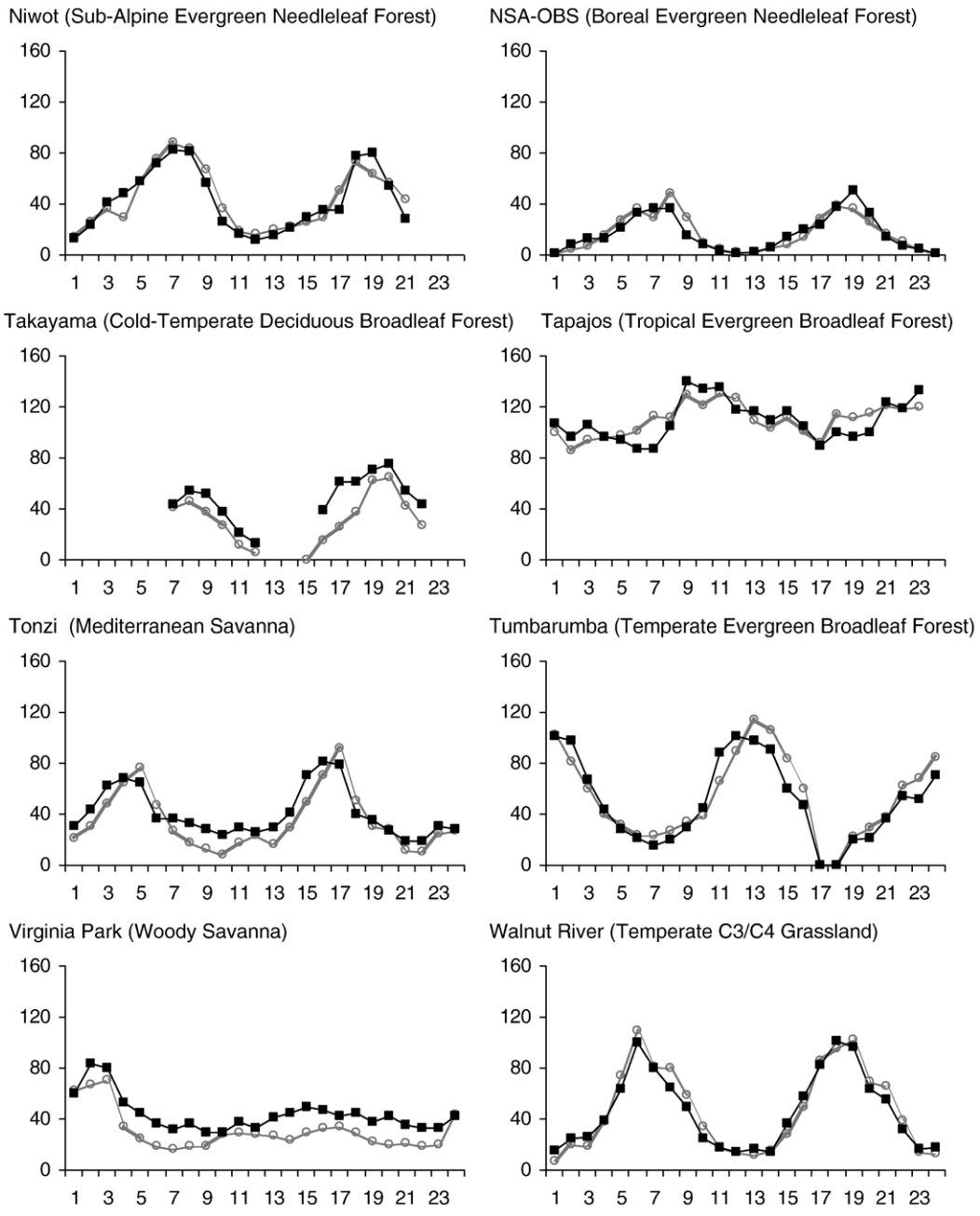

Fig. 4 (*continued*).

2.4. Uncertainty analysis

Uncertainty in the outputs are estimated from the model with the method of moments (Hansen, 1982), which stems from Gaussian error propagation, and is also known as the boundary element method, the surface integral equation method, and the Galerkin or Galerkin–Petrov method for surface integral equations (Warnick & Chew, 2004). The method of moments estimators are obtained from the sample mean and the sample variance of the exceedances (e.g., Madsen et al., 1997). Although Maximum Likelihood is easier to use and more efficient, given the known underlying distribution the method of moments is an exact measure of accuracy in comparison with Monte Carlo and other approximate methods that are dependent on the number of simulations run (e.g., Rushdi & Kafrawy, 1988). Uncertainty in LE is the propagation of the partial derivatives of the input parameters and their respective covariances, where x and y are the 5 inputs R_n, NDVI, SAVI, T_{max}, and ea:

$$s_{LE} = \sqrt{\sum\left(\left(\frac{\partial LE}{\partial x}s_x\right)^2 + 2r_{xy}\left(\frac{\partial LE}{\partial x}s_x\right)\left(\frac{\partial LE}{\partial y}s_y\right)\right)} \quad (1)$$

We used the method of moments to determine the sensitivity of our model to variation in each of the input parameters. The

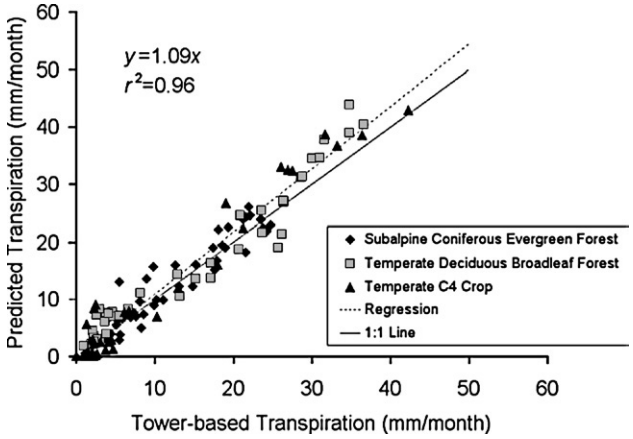

Fig. 5. Testing the model estimates of transpiration against the tower-based energy balance partitioning estimates in three contrasting ecosystem types. Shown are the 8-day means of daytime fluxes ($W \cdot m^{-2}$) for 1 year at each site.

method of moments is particularly useful when the error in the input data is known, as in the case of flagged anomalous data or uncertainty associated with interpolation/extrapolation (e.g., cloudy pixels) or gap filling (e.g., measurement failure).

3. Results

3.1. FLUXNET validation

The results for predicted LE based on our model versus measured LE show good agreement at all 16 FLUXNET sites (Fig. 3). The r^2 for all sites is 0.90, though the fit varies from site to site (Table 4 and Fig. 4); the RMSE is 16 mm/month. Data in Fig. 3 are shown as monthly means (to correspond with ISLSCP-II monthly data for the following global analysis). The model accounted for 94% of the variation in cumulative LE ($mm \cdot yr^{-1}$) with a RMSE of 12 $mm \cdot yr^{-1}$, or 13% of the observed mean. Further, systematic differences between model predictions were minimal ($RMSE_s = 5\ mm \cdot yr^{-1}$), with nearly all of the model error (96%) related to unsystematic differences ($RMSE_u = 11\ mm \cdot yr^{-1}$). $RMSE_s$ and $RMSE_u$ were calculated following Willmott (1982). Based on these results, the model appears to be relatively accurate ($+/-4\ mm \cdot yr^{-1}$) with a precision – or the ability to resolve differences between sites and between years – of 68 $mm \cdot yr^{-1}$.

The 16 sites represent a wide range of land covers, climates, fluxes and eddy covariance footprints. The model overpredicted LE at three sites—Takayama ($y = 0.91x + 17.07$; $r^2 = 0.78$), Tonzi ($y = 0.78x + 13.96$; $r^2 = 0.83$), and Virginia Park ($y = 0.83x + 18.17$; $r^2 = 0.81$). The Takayama estimates were problematic due to missing data. The Tonzi results were vulnerable to a lag in the seasonal patterns of NDVI and SAVI relative to LE. Our Virginia Park estimates compare to the r^2 of 0.74 by Cleugh et al.'s (2007) evaporation model for the site (and to the Tumbarumba site—our $r^2 = 0.89$ to their 0.88), although advection creates a problem with f_{SM} at this site. The Tapajos r^2 is low (0.55) not due to overprediction, but to lack of LE variation at this site—LE is nearly constant year-round so any slight deviation in the model estimate drops the r^2 substantially.

The energy balance partitioning approach provided estimates of LE_c (and LE_s) that were consistent with those based on sap flow measurements of transpiration ($r^2 = 0.66$, RMSE = 99 $W \cdot m^{-2}$). The slope and intercept of the regression line between the tower-based energy balance partitioning estimates and observed canopy transpiration were not significantly different from 1 and 0, respectively ($P = 0.05$). For soil evaporation, the slope and intercept were significantly different from 1 and 0 (data not shown), however, these differences must be considered in context of the large average uncertainty of the observations (>20%, based on Ham et al., 1990). Model estimates of transpiration slightly overestimated those based on the tower (subalpine coniferous evergreen forest, temperate deciduous broadleaf forest, temperate C4 crop) energy balance partitioning method (Fig. 5), with a slope of 1.09 and an intercept not significantly different from zero ($P = 0.05$).

3.2. Uncertainty analysis

Two problems are associated with the eddy flux validation: pixel-to-footprint mismatch and eddy flux energy balance closure. First, we used 1-km^2 MODIS NDVI pixels for amorphous polygon eddy flux footprints that change throughout the day and year. If the vegetation and environmental characteristics within the footprint are representative of the surrounding area in which the MODIS pixels contain, then the pixel-to-footprint match should be adequate. A forested eddy flux site adjacent to a clear cut, for example, would provide NDVI problems if both the forest and clear cut were included in the MODIS overlap. Thus, some error in our model estimates for the eddy flux sites can be attributed to inaccurate NDVI estimates for the footprints. Temporally, the link between instantaneous overhead passes with daily integrated fluxes must be addressed. With regards to eddy flux CO_2, Sims et al. (2005) has shown, and we have confirmed with our own data, that the CO_2 flux taken at 2 pm scales with the daily integral. The same question is raised for variables used to assess LE. The strength of our approach lies in estimating the evaporative fraction, as argued by Nishida et al. (2003), which is generally constant throughout the day. The challenge thus remains with remote sensing of the daily integrals of R_n, a separate but equally important issue than that of the accuracy of the model itself.

Second, our validation is dependent on the accuracy of the eddy flux LE measurements, but energy balance closure at these sites is imperfect due to complexity in wind variation, footprint representation, and sampling variability (Wilson et al., 2002). The eddy flux sites generally achieve about 90% closure with

Table 5
Cross-correlations between ISLSCP-II global input parameters for 1993

r^2	NDVI	R_n	T_{max}	ea
NDVI		0.03	0.85	0.97
R_n			0.17	0.05
T_{max}				0.92
ea				

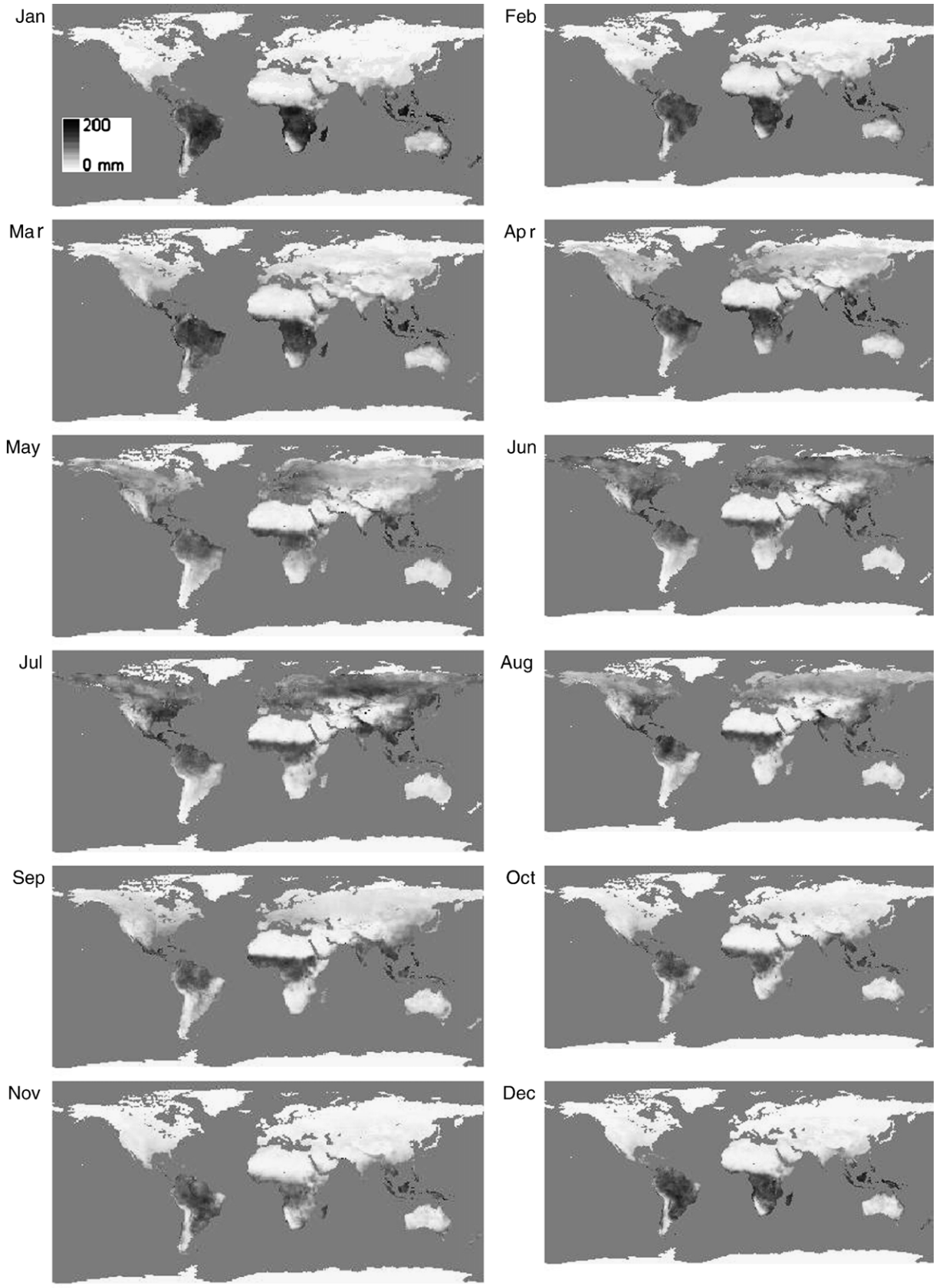

Fig. 6. Month-to-month variation in LE for 1993.

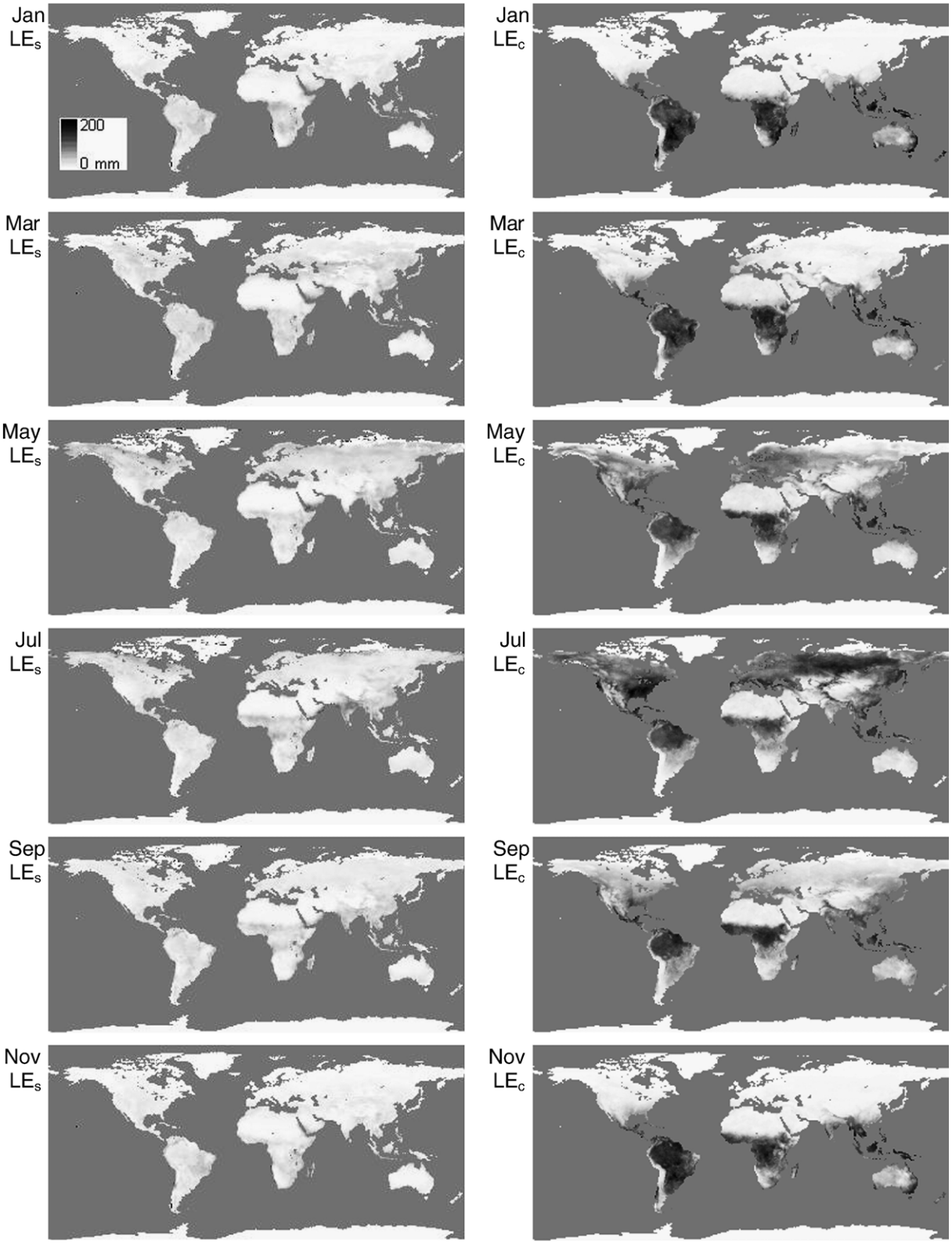

Fig. 7. Soil evaporation (LE_s) and canopy transpiration (LE_c) bi-monthly for 1993.

10% of the variation unexplained. Therefore, the best model would subsequently explain only an r^2 of around 0.90, which is generally what our model produces.

The certainty of the model outputs result depends largely on the certainty of the input data. To execute the method of moments we first calculated the cross-correlations between the input

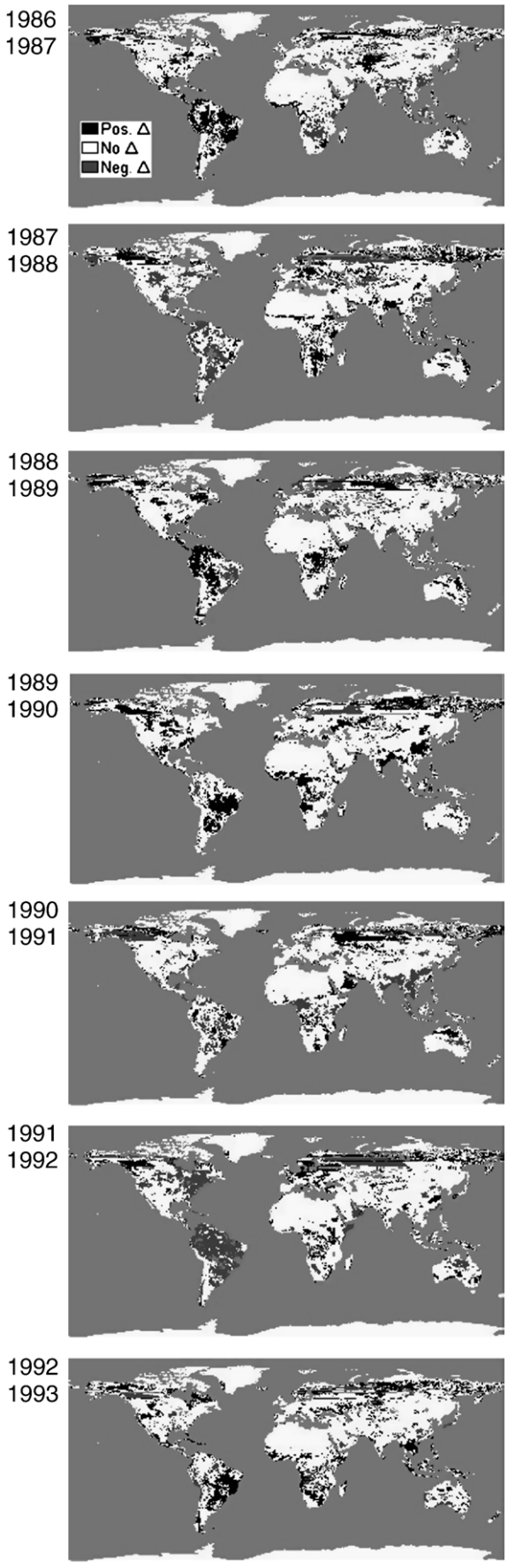

parameters (Table 5). Associations with SAVI were equivalent to those with NDVI, so we report uncertainty only in NDVI. The cross-correlations were highest among NDVI and T_{max}, NDVI and ea, and T_{max} and ea. Next, we determined the error within the four inputs. The uncertainty varies spatially from pixel-to-pixel and region-to-region, and temporally from month-to-month and year-to-year, but we standardized the uncertainty assessment by testing our model by propagating uniform errors of 10% and 25% for each of the four input parameters. A 10% error in the mean of the four inputs propagates through our model for a mean error of 11.3%. At 25% error in the mean of the four inputs, our model is in error at 28.3%.

Next we varied the error of only one input at a time, while holding the error constant for the other inputs. For example, we assumed that we had zero error in all of the inputs except R_n, which had 10% error. We ran the Method of Moments in each case to see what the final error was. Then, we assumed we had zero error in all of the inputs except NDVI, which had 10% error, and so on. The major result of the uncertainty analysis is that our model is heavily dependent on the accuracy of the R_n input data, as error in R_n contributes to the bulk of the model error; NDVI is second in total error contribution, followed by minimal error from T_{max} and ea. Errors in T_{max} and ea have minimal influence in our model because we treat these variables in a relative sense for ecophysiological constraints—our model is primarily dependent on the error associated with R_n. For instance, ea, which is used for RH and f_{wet}, follows the transition between wet and dry LE, but LE will never go beyond potential LE regardless of how ea varies (also, RH as an inherent relative term is constrained in range by its own definition). R_n, on the other hand, dictates the magnitude of potential LE. Also, NDVI helps to partition R_n into R_{ns} and R_{nc}. Thus, while the uncertainty analysis may suggest a linear dependency of the final error on that in each parameter, the bulk of the error, in fact, is dependent on R_n and to a lesser extent NDVI, but not T_{max} and ea.

3.3. Global analysis

We assessed the global spatial and temporal patterns of LE from 1986–1993 using 1° monthly gridded ISLSCP-II input data. The month-to-month pattern for 1993 shows the seasonal shifts (Fig. 6). The southern hemispheric tropics remain consistently high throughout the year, while the major deserts of northern Africa and Australia remain consistently low. The major global change on a monthly scale occurs in the high northern latitudes, where LE shows high variation with increases into the northern summer while tapering off into the winter.

Our model partitions LE into LE_s, LE_c and LE_i; the partitioning of LE is shown in Fig. 7 bi-monthly for 1993. LE_i averages 23% of total LE from 30°S–30°N, but is relatively

Fig. 8. Year-to-year change in LE. Gray land areas indicate a negative change between years (<10 mm), and black areas indicate an increase in evapotranspiration (>10 mm). White areas represent no change, or within two standard deviations around a mean of 0.

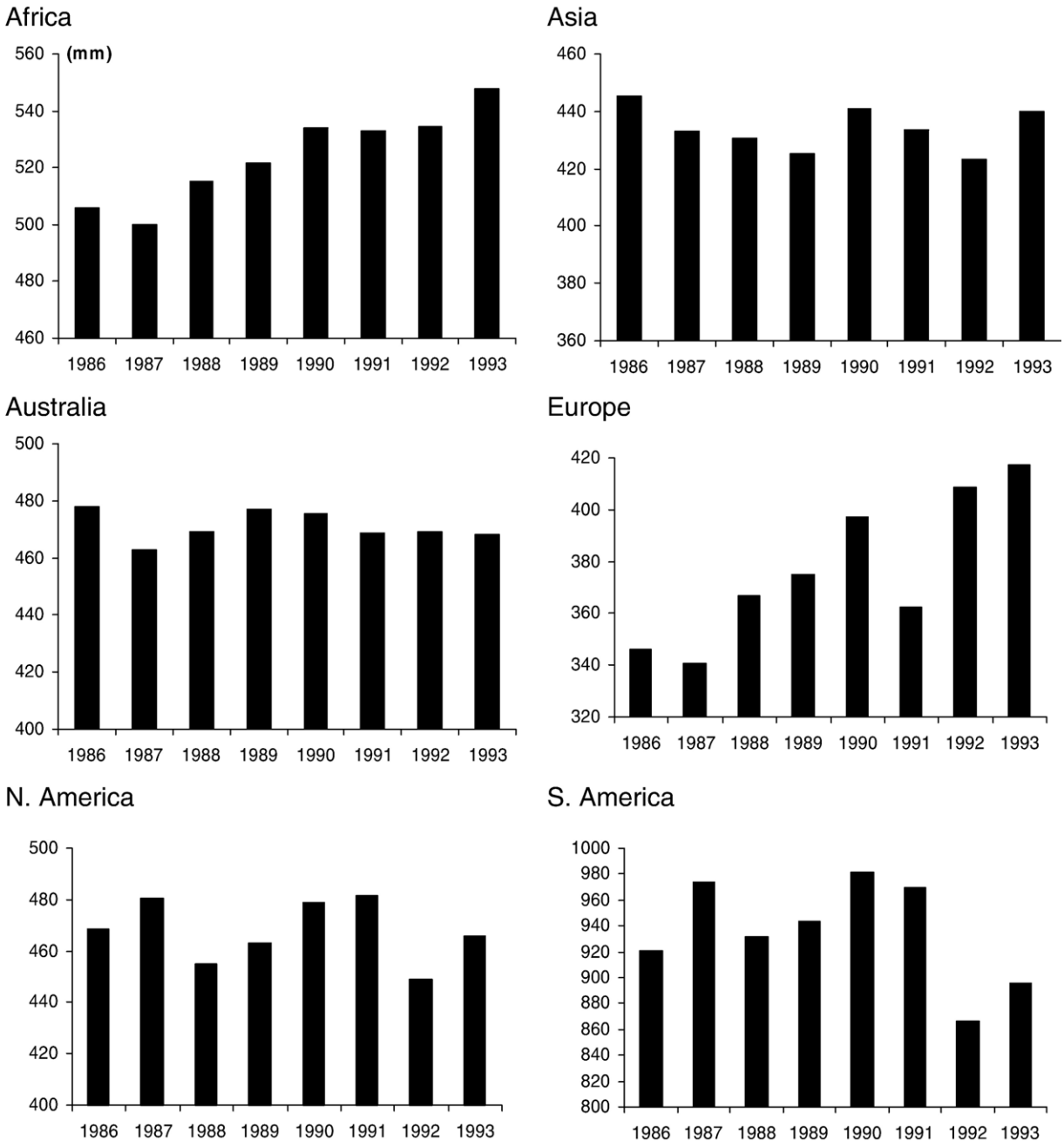

Fig. 9. Continental averages of total LE (mm) per year.

minimal outside of the tropics (<4%). LE_s and LE_c tend to complement or offset each other. In the Amazon LE_s is predicted to be low because of the high canopy cover, and hence high canopy evaporation contribution to LE. In the northern latitudes, LE_s becomes active before LE_c as seen in the March–May figures, though LE_c takes over in the middle of the summer. In the Indian sub-continent LE_s is the major contributor to LE due largely to irrigation particularly in the summer, and LE_c is minimal throughout the year here. LE_s and LE_c increase towards the equator into the summer throughout Africa south of the Sahara. LE_c is minimal in the Sahara and Australian Outback deserts, though LE_s can be relatively high at certain times of the year.

The year-to-year changes in mean annual LE from 1986 to 1993 showed distinct spatial patterns and a cyclical nature (Fig. 8). From 1986–1987, LE increased primarily in the Amazon and in western Asia, while it decreased in southern Africa. The reverse occurred from 1987–1988, where S. America and western Asia experienced a decrease in LE and southern Africa an increase; LE increased in eastern Europe.

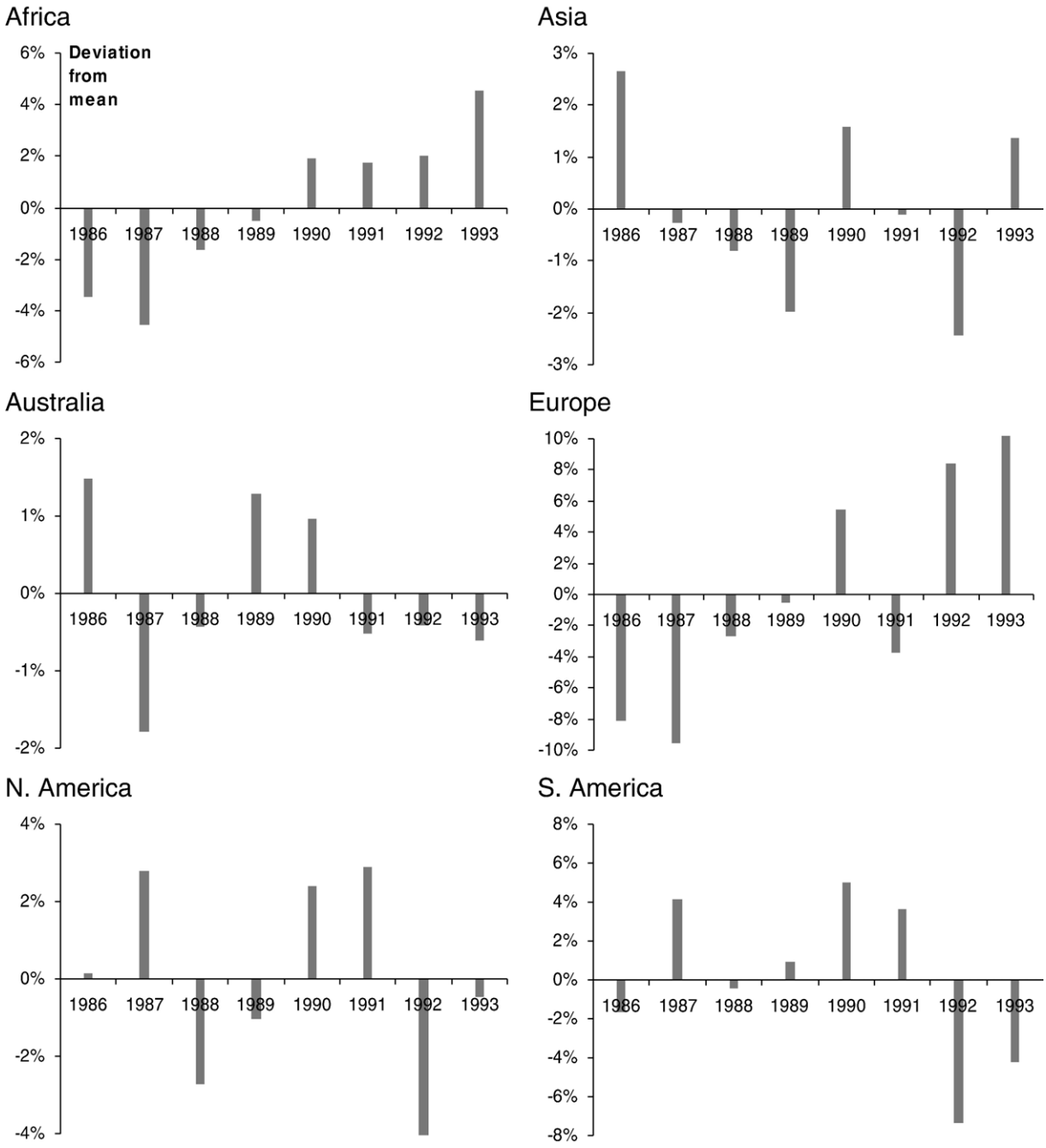

Fig. 10. Continental deviation from the mean LE (mm) for the 8-year time period per year.

LE increased in S. America and central Africa from 1988–1989 and 1989–1990, although it decreased in eastern Brazil from 1988–1989; LE increased in Eastern India and China from 1989–1990. Eastern India and China, along with the Congo, decreased in LE from 1990–1991; pockets of the Middle East and Australia showed increases in LE. From 1991–1992, major decreases in LE were present throughout S. America and northeastern N. America. LE increased in S. America, southern Africa and southeast Asia from 1992–1993.

Continentally, LE showed only minor fluctuations from the mean for the time period except for Europe, which ranged from 340 to 420 mm over the 8 years (Figs. 9 and 10). S. and N. America had marked drops in LE in 1992. Africa showed a steady rising trend in LE from 1986–1993. The lowest variances were in Australia and Asia, while the highest were in Europe and S. America. S. America dominates the continental LE at roughly double that from each of the other continents. The annual global sum of LE increased over the 8-year time period, although the correlation is low (Fig. 11). LE

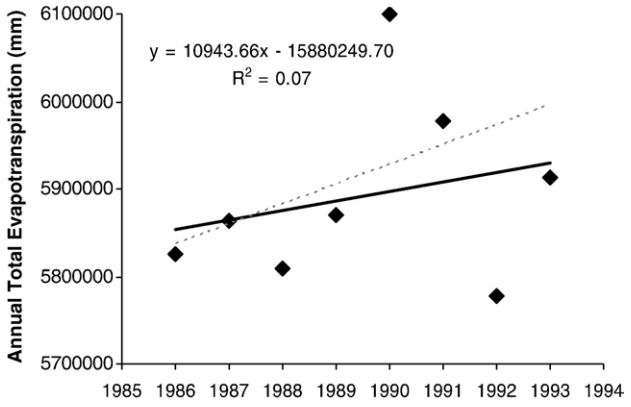

Fig. 11. Global annual sum of LE (mm) for the 8-year time period per year. The dashed line is the best-fit with year 1992 removed.

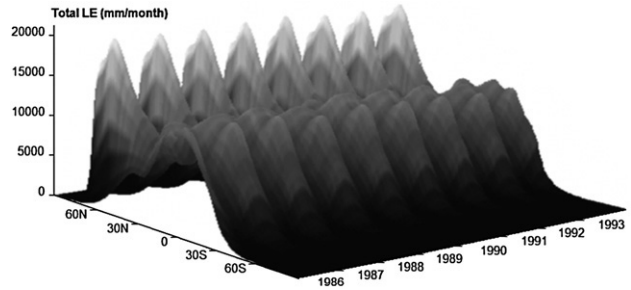

Fig. 13. Annual total LE for 1986–1993 as the average across latitudinal bands.

for year 1992 was uncharacteristically low due to a dimming effect from the Mt. Pinatubo eruption in 1991 (e.g., Hansen et al., 1992). Removal of year 1992 gives an r^2 of 0.29. Although year 1990 had the highest global LE, this year was not the highest year for any of the continents other than for S. America, which is the major contributor to global LE (Fig. 9).

Although global validation is problematic, we are able to compare our model with other global models from the literature (Baumgartner & Reichel, 1975; Budyko, 1978; Choudhury et al., 1998; Henning, 1989; Mintz & Walker, 1993; Pike, 1964). Our global annual total LE as averaged across latitudinal bands falls directly in line with the other published results (Fig. 12). We include as reference for comparison R_n, the original potential LE from Priestley and Taylor (1972), precipitation (PPT) from ISLSCP-II, and an aridity index—LE=PPT/sqrt(1+(PPT/PET)^2). Evaporative fraction can be calculated by dividing LE by R_n ($-G$). Our unconstrained model is equivalent to Priestley and Taylor (1972). The most important constraint is f_{SM} in reducing potential to actual LE because f_{SM} dictates the soil water limitation, followed by f_g, f_M, and finally f_T. We show data for 1986 in this comparison figure, and all of our years show a similar pattern. Fig. 12 can be stretched 3-dimensionally ("flying carpet") across all the years in our dataset (Fig. 13). The annual sum averaged latitudinally tends to remain relatively consistent from year to year within a latitudinal band. Seasonally, the annual sum can be split 3-dimensionally into monthly, latitudinally-averaged values of LE (Fig. 14). The equatorial latitudes tend to remain consistently high throughout the year. The southern and northern hemispheres display the seasonal phase offset where the northern hemisphere increases in LE in their summer in synch with the southern hemisphere decrease in their winter and vice versa.

Specific biomes and climatic areas are more sensitive to uncertainties in some input parameters than others due to variability between parameters (e.g., Mediterranean sites to T_{max}). We evaluated the per-pixel variation in the ISLSCP-II input parameters to our model with the method of moments to produce a global map of uncertainty in our global LE estimates (Fig. 15). Lighter areas represent areas of high certainty, whereas darker areas represent areas of high uncertainty. Data shown in Fig. 15 are for the average uncertainty for 1993. The largest area of uncertainty results from the high northern latitudinal striping, though spot areas/pixels occur throughout some of the continental edges due generally to

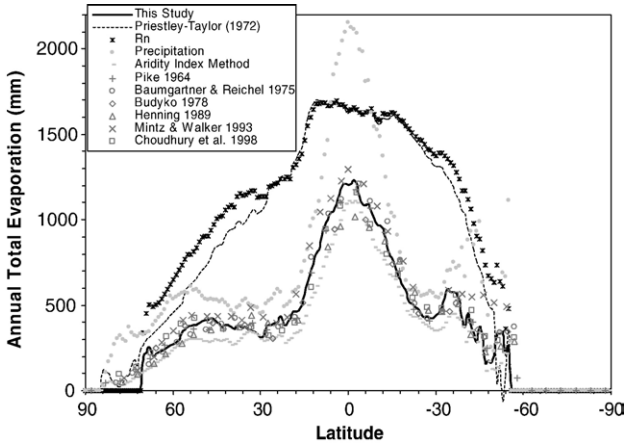

Fig. 12. Annual total LE for year 1986 (for comparison) as the average across latitudinal bands (90°N to −90°S).

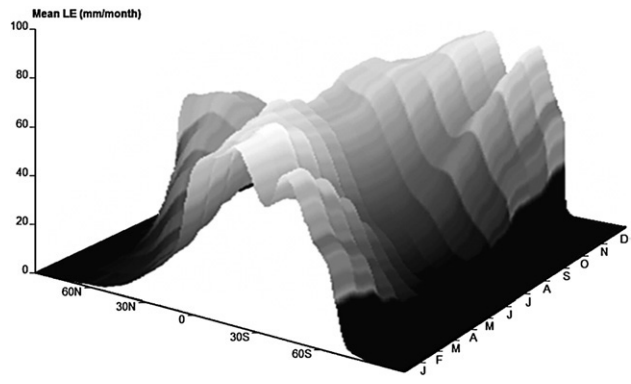

Fig. 14. .Monthly total LE as the average across latitudinal bands across year 1993.

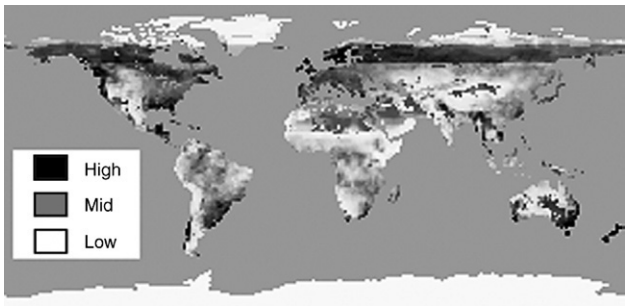

Fig. 15. Method of Moments global output based on variability within ISLSCP-II input parameters for 1993. Lighter areas represent low uncertainty and darker areas represent high uncertainty within the range of LE values.

missing pixels. Most areas fall within a mid-to low-range of uncertainty.

4. Discussion

Major global climatic perturbations and influences, such as El Niño Southern Oscillation (SOI > 0.5), La Niña (SOI < −0.5), and volcanic eruptions such as Mt. Pinatubo in 1991, have caused alterations in the global water cycle and in the land–atmosphere water flux. In 1987 El Niño led to the highest rates of LE for N. America and second highest for S. America for our dataset (Fig. 9). At the same time, Australia, Africa and Europe experienced their lowest rates of LE. The following La Niña in 1988 led to a reversal-N. and S. America dropped their rates of LE considerably, while Australia, Africa and Europe rebounded for significant increases. In 1991, the Mt. Pinatubo eruption, which was the second largest volcanic eruption of the century, caused many climatic anomalies (e.g., Hansen et al., 1992) and may have had a mediating influence on the effects of the following El Niño (Self et al., 1997). Following the Mt. Pinatubo eruption, year 1992 had the largest drops in LE for Asia, N. and S. America for our dataset due to a dimming effect and subsequent reduction in R_n. Europe, however, had the second largest gain in LE in 1992.

There are two problems with the ISLSCP-II R_n. First is the high northern latitudinal striping that occurs in the winter months (also occurs in the southern hemisphere, but not over land). Although one can assume that LE is minimal when R_n is undetectable, our model still predicts high uncertainty for these missing data (Fig. 15). The second problem occurs only in year 1987, and only in S. America. A curved differentiation of R_n cuts through the middle of S. America, which caused the Amazon to be split into two sections. This problem in particular must be remedied for further application of the 1987 SRB/ISLSCP-II R_n.

We are confident in the relative trends and absolute pixel values in the global products from our model, but any estimates smaller (sub-pixel) and larger (continental) contain some caveats. Sub-grid variability is so large that to derive particular site information from the 1° pixels could lead to large errors. Continental validation with PPT and runoff data is also possible, but unknown storage-to-LE partitioning and upscaling of runoff stream data to 1° pixels becomes problematic. ISLSCP-II provides runoff data, but explicitly states that these data are not recommended for model validation because the runoff data are based on a combination of model estimates and discharge measurements. Model runs at finer time scales require well-characterized input means from continuous data. We also hesitate to report model estimates for very small spatial scales, such as at the tree or leaf levels. At these scales, parameters that are not included in our model, such as wind speed, become much more tightly coupled to LE (Jarvis & McNaughton, 1986; McNaughton & Jarvis, 1991). In the northern hemisphere, the continental sums are subject to interference from winter striping. Generally, we assumed values of striping to be close to zero, but these estimates are subject to the accuracy of the assumption.

Moving from one scale to the next, whether spatially or temporally is of considerable interest, especially with regards to modeling fluxes such as LE (Su et al., 2007). A more "scalable" model should include not only more parameters (e.g., leaf-level properties), but also de-coupling coefficients (Jarvis & McNaughton, 1986; McNaughton & Jarvis, 1991) attached to each parameter weighting them differently as one moves across scales. With our model, the smallest spatial scale we validate at is the eddy covariance tower footprint, but it is possible that the model works well at smaller spatial scales. We make a big jump to the 1° ISLSCP-II pixel scale without changing the model at all-but do we need to change the model? Comparing with a wide range of global models (Fig. 12), our model compares favorably. Therefore, we can postulate that the influences of the inputs at the ecosystem scale are similar to that at the global scale. Temporally, we report estimates at the monthly scale, but the model can be run at smaller and larger temporal scales as well. Our model, however, requires a certain temporal scale-specific response in the vegetation to water deficits (i.e., LAI, SAVI, NDVI). Further, defining the temporal scale at which parameters such as f_{wet} operate is implicit in the calculations.

Based on >1200 observations of PPT and runoff, Budkyo (Budyko, 1948; Budyko, 1951; Budyko, 1971; Budyko & Zubenok, 1961) found that the relationship between annual LE and the humidity index (PPT/PET) fell between the empirical models of Schreiber (1904) and Ol'dekop (1911). Essentially, the wetter it is (the higher the humidity index PPT/PET) the higher the AET, but the relationship is nonlinear. Budyko simply solved for the geometric mean of Schreiber (1904) and Ol'dekop (1911). Turc (1954) proposed a similar formula using Thornthwaite's approach based on 250 independent catchments in different climate regimes. Pike (1964) followed with a PET estimation using Penman's approach. In essence, all of these models describe a transition from water to energy limitation on LE as PPT/AET increases (as it gets wetter).

Our ecophysiological model of the Priestley–Taylor method relies on surface changes as defined by R_n, NDVI, SAVI, T_{max}, and ea, all of which can be acquired fully from remote sensing. Recently, Bisht et al. (2005) developed a method to estimate R_n solely from MODIS. Compared with observed measurements from their study sites, correlation coefficients ranged from 0.85 (daily average) to 0.90 (instantaneous); RMSE's were 60 and 74 $W \cdot m^{-2}$, respectively. Irmak et al. (2003) introduced an

equation to measure R_n based on minimum and maximum air temperature, incoming solar radiation, and distance between the Earth and sun. They report coefficients of determination across eight validation sites between 0.96–0.99. Many studies have compared air temperature from satellite sensors to surface measurements across a wide range of land covers (Bisht et al., 2005; Czajkowski et al., 1997; Goetz et al., 1995; Houborg & Soegaard, 2004; Jin et al., 1997; Kalluri & Dubayah, 1995; Lakshmi et al., 2002; Lakshmi & Susskind, 2000; Prince et al., 1998). Error in satellite-based air temperature has been reported as 4 °C from AVHRR (e.g., Lakshmi et al., 2002; Prince et al., 1998). Vegetation indices such as NDVI or SAVI are direct products of band calculations. Steven et al. (2003) report NDVI and SAVI differences for 15 different satellite sensors, including MODIS and AVHRR. Their results showed that the vegetation indices can be interconverted to a precision of 1–2% across all sensors for both vegetation indices. Proxies for satellite-based estimates of ea have been reported from MODIS and AVHRR (Czajkowski et al., 2002; Houborg & Soegaard, 2004; Motell et al., 2002; Sobrino & El Kharraz, 2003). Motell et al. (2002) report a RMSE of 3.8 mm (R=0.91) for precipitable water vapor – which can be converted to ea (Choudhury, 1998; Smith, 1966) – satellite estimates based on Dalu (1986) over Hawaii from AVHRR. Czajkowski et al. (2002) showed that near-surface water vapor could be estimated with AVHRR or MODIS with a correlation of 0.36 as compared to BOREAS ground measurements, though they explain the low r^2 values as a result of spatial and temporal mismatches between surface and satellite measurements.

Our next step is to run our model finer spatial and temporal scales using solely remote sensing data (e.g., global MODIS 1-km^2 data). Currently, the model performs well across a wide variety of ecosystems, vegetation types, footprints, and climatic regimes. It is also simple enough so that it can potentially be run solely with remote sensing inputs, and global estimates are easily producible. We have assessed the uncertainty within our model based on the error associated with the input data, and we are confident in the absolute values of LE at an ecosystem scale and in the relative trends of LE at the global scale. Our model can be integrated straightforwardly into larger process models of global climate change, water balance, net primary productivity, floods and droughts, and irrigation.

Acknowledgments

The authors thank G. Biging, T. Dawson, J. Lee, Y. Malhi, Y. Ryu and E. Walker for support and assistance with this project; C. Levitan provided programming support. Four anonymous reviewers provided useful comments and insightful suggestions to this manuscript. We thank the many FLUXNET site investigators for allowing us to use their tower eddy flux data for the model validation: R. Coulter, A. Granier, D. Hollinger, A. Knohl, P. Lafleur, R. Leuning, T. Martin, J. Moncrieff, R. Monson, T. Myers, H. Schmid, S. Wofsy, and S. Yamamoto. The authors wish to thank the Distributed Active Archive Center (Code 902.2) at the Goddard Space Flight Center, Greenbelt, MD, 20771, for producing the AVHRR data in their present form and distributing them. The original AVHRR data products were produced under the NOAA/NASA Pathfinder program, by a processing team headed by Ms. Mary James of the Goddard Global Change Data Center; and the science algorithms were established by the AVHRR Land Science Working Group, chaired by Dr. John Townshend of the University of Maryland. Goddard's contributions to these activities were sponsored by NASA's Mission to Planet Earth program. J. Fisher was supported by NASA Headquarters under the Earth System Science Fellowship Grant NGT5-30473, and from a University of California, Berkeley Faculty Research Grant.

References

Baldocchi, D., & Meyers, T. (1998). On using eco-physiological, micrometeorological and biogeochemical theory to evaluate carbon dioxide, water vapor and trace gas fluxes over vegetation: A perspective. *Agricultural and Forest Meteorology*, *90*, 1–25.

Baldocchi, D., Falge, E., Gu, L. H., Olson, R. J., Hollinger, D., Running, S. W., et al. (2001). FLUXNET: A new tool to study the temporal and spatial variability of ecosystem-scale carbon dioxide, water vapor, and energy flux densities. *Bulletin of the American Meteorological Society*, *82*, 2415–2434.

Baldocchi, D., Hicks, B., & Meyers, T. (1988). Measuring biosphere–atmosphere exchanges of biologically related gases with micrometeorological methods. *Ecology*, *69*, 1331.

Barton, I. J. (1979). A parameterization of the evaporation from nonsaturated surfaces. *Journal of Applied Meteorology*, *18*, 43–47.

Baumgartner, A., & Reichel, E. (1975). *The world of water balance.* New York: Elsevier.

Beer, A. (1852). Bestimmung der Absorption des rothen Lichts in farbigen Flüssigkeiten. *Ann. Phys. u. Chem*.

Bisht, G., Venturini, V., Islam, S., & Jiang, L. (2005). Estimation of the net radiation using MODIS (Moderate Resolution Imaging Spectroradiometer). *Remote Sensing of Environment*, *97*, 52–67.

Black, T. A. (1979). Evapotranspiration from Douglas-fir stands exposed to soil water deficits. *Water Resources Research*, *15*, 164–170.

Bouchet, R. J. (1963). Evapotranspiration re´elle evapotranspiration potentielle, signification climatique. *Int. Assoc. Sci. Hydrol.* (pp. 134–142).

Bouguer, P. (1729). *Traite'd'optique sur la gradation de la lumiere.*

Budyko, M. I. (1948). *Evaporation under natural conditions.* Leningrad: Gidrometeoizdat.

Budyko, M. I. (1951). On the influence of reclamation measures upon potential evapotranspiration. *Izv. Akad. Nauk. SSSR Ser. Geogr.*, *Vol. 1* (pp. 16–35).

Budyko, M. I. (1971). *Climate and life* (pp. 472). Leningrad: Hydrometeoizdat.

Budyko, M. I. (1978). The heat balance of the Earth. In J. Gribbin (Ed.), *Climatic change* (pp. 85–113). New York: Cambridge University Press.

Budyko, M. I., & Zubenok, L. I. (1961). The determination of evaporation from the land surface. *Izv. Ak. Nauk SSR, Se. Geog.*, *Vol. 6* (pp. 3–17).

Campbell, G. S., & Norman, J. M. (1998). *An introduction to environmental biophysics* (pp. 286). New York: Springer-Verlag.

Choudhury, B. J. (1997). Global pattern of potential evaporation calculated from the Penman–Monteith equation using satellite and assimilated data. *Remote Sensing of Environment*, *61*, 64–81.

Choudhury, B. J. (1998). Estimation of vapor pressure deficit over land surfaces from satellite observations. *Advances in Space Research*, *22*, 669–672.

Choudhury, B. J., & DiGirolamo, N. E. (1998). A biophysical process-based estimate of global land surface evaporation using satellite and ancillary data I. Model description and comparison with observations. *Journal of Hydrology*, *205*, 164–185.

Choudhury, B. J., DiGirolamo, N. E., Susskind, J., Darnell, W. L., Gupta, S. K., & Asrar, G. (1998). A biophysical process-based estimate of global land surface evaporation using satellite and ancillary data II. Regional and global patterns of seasonal and annual variations. *Journal of Hydrology*, *205*, 186–204.

Choudhury, B. J., Idso, S. B., & Reginato, R. J. (1987). Analysis of an empirical model for soil heat flux under a growing wheat crop for estimating evaporation by infrared-temperature based energy balance equation. *Agricultural and Forest Meteorology*, *39*, 283−297.

Cleugh, H. A., Leuning, R., Mu, Q., & Running, S. W. (2007). Regional evaporation estimates from flux tower and MODIS satellite data. *Remote Sensing of Environment*, *106*, 285−304.

Clothier, B. E., Clawson, K. L., Pinter, P. J., Moran, M. S., Reginato, R. J., & Jackson, R. D. (1986). Estimating of soil heat flux from net radiation during the growth of alfalfa. *Agricultural and Forest Meteorology*, *37*, 319−329.

Czajkowski, K. P., Goward, S. N., Shirey, D., & Walz, A. (2002). Thermal remote sensing of near-surface water vapor. *Remote Sensing of Environment*, *79*, 253−265.

Czajkowski, K. P., Mulhern, T., Goward, S., Cihlar, J., Dubayah, R., & Prince, S. (1997). Biospheric environmental monitoring at BOREAS using AVHRR observations. *Journal of Geophysical Research*, *102*, 29651−29662.

Dalu, G. (1986). Satellite remote sensing of atmospheric water vapour. *International Journal of Remote Sensing*, *7*, 1089−1097.

Daughtry, C. S. T., Kustas, W. P., Moran, M. S., Pinter, P. J., Jackson, R. D., Brown, P. W., et al. (1990). Spectral estimates of net radiation and soil heat flux. *Remote Sensing of Environment*, *32*, 111−124.

Davies, J. A., & Allen, C. D. (1973). Equilibrium, potential and actual evaporation from cropped surfaces in southern Ontario. *Journal of Applied Meteorology*, *12*, 649−657.

De Bruin, H. A. R., & Holtslag, A. A. M. (1982). A simple parameterization of the surface fluxes of sensible and latent heat during daytime compared with the Penman–Monteith concept. *Journal of Applied Meteorology*, *21*, 1610−1621.

De Bruin, H. A. R., & Stricker, J. N. M. (2000). Evaporation of grass under non-restricted soil moisture conditions. *Hydrological Sciences Journal*, *45*, 391−406.

Denmead, O. T. (1976). Temperature cereals. In J. L. Monteith (Ed.), *Vegetation and the atmosphere* (pp. 1−32). London: Academic Press.

Eichinger, W. E., Parlange, M. B., & Stricker, H. (1996). On the concept of equilibrium evaporation and the value of the Priestley–Taylor coefficient. *Water Resources Research*, *32*, 161−164.

Entekhabi, D., Asrar, G. R., Betts, A. K., Beven, K. J., Bras, R. L., Duffy, C. J., et al. (1999). An agenda for land surface hydrology research and a call for the second international hydrological decade. *Bulletin of the American Meteorological Society*, *80*, 2043−2058.

Federer, C. A., Vörösmarty, C., & Fekete, B. (2003). Sensitivity of annual evaporation to soil and root properties in two models of contrasting complexity. *Journal of Hydrometeorology*, *4*, 1276−1290.

Federer, C. A., Vörösmarty, C. J., & Fekete, B. (1996). Intercomparison of methods for calculating potential evaporation in regional and global water balance models. *Water Resources Research*, *32*, 2315−2321.

Fisher, J. B., Debiase, T. A., Qi, Y., Xu, M., & Goldstein, A. H. (2005). Evapotranspiration models compared on a Sierra Nevada forest ecosystem. *Environmental Modelling & Software*, *20*, 783−796.

Flanagan, L. B., Wever, L. A., & Carlson, P. J. (2002). Seasonal and interannual variation in carbon dioxide exchange and carbon balance in a northern temperate grassland. *Global Change Biology*, *8*, 599−615.

Flint, A. L., & Childs, S. W. (1991). Use of the Priestley–Taylor evaporation equation for soil water limited conditions in a small forest clearcut. *Agricultural and Forest Meteorology*, *56*, 247−260.

Gao, X., Huete, A. R., Ni, W. G., & Miura, T. (2000). Optical–biophysical relationships of vegetation spectra without background contamination. *Remote Sensing of Environment*, *74*, 609−620.

Giles, D. G., Black, T. A., & Spittlehouse, D. L. (1984). Determination of growing season soil water deficits on a forested slope using water balance analysis. *Canadian Journal of Forest Research*, *15*, 107−114.

Goetz, S. J., Halthore, R., Hall, F. G., & Markham, B. (1995). Surface temperature retrieval in a temperature grassland with multi-resolution sensors. *Journal of Geophysical Research*, *100*, 25397−25410.

Goldstein, A. H., Hultman, N. E., Fracheboud, J. M., Bauer, M. R., Panek, J. A., Xu, M., et al. (2000). Effects of climate variability on the carbon dioxide, water, and sensible heat fluxes above a ponderosa pine plantation in the Sierra Nevada (CA). *Agricultural and Forest Meteorology*, *101*, 113−129.

Gordon, L. J., Steffen, W., Jonsson, B. F., Folke, C., Falkenmark, M., & Johannessen, A. (2005). Human modification of global water vapor flows from the land surface. *Proceedings of the National Academy of Sciences of the United States of America*, *102*, 7612−7617.

Granier, A., Biron, P., & Lemoine, D. (2000). Water balance, transpiration and canopy conductance in two beech stands. *Agricultural and Forest Meteorology*, *100*, 291−308.

Hall, F. G., Collatz, G. J., Los, S. O., Brown, E., Colstoun, D. E., & Landis, D. (2005). *ISLSCP Initiative II: DVD/CD-ROM: NASA.*

Ham, J. M., Heilman, J. L., & Lascano, R. J. (1990). Determination of soil water evaporation and transpiration from energy balance and stem flow measurements. *Agricultural and Forest Meteorology*, *52*, 287−301.

Hansen, L. P. (1982). Large sample properties of generalized method of moments estimators. *Econometrica*, *50*, 1029−1054.

Hansen, J., Lacis, A., Ruedy, R., & Sato, M. (1992). Potential climate impact of Mount-Pinatubo eruption. *Geophysical Research Letters*, *19*, 215−218.

Hare, F. K. (1980). Long-term annual surface heat and water balances over Canada and the United States south of 60 N: Reconciliation of precipitation, run-off and temperature fields. *Atmosphere-Ocean*, *18*, 127−153.

Henning, D. (1989). *Atlas of the surface heat balance of the continents.* Berlin: Gebruder Borntraeger.

Hollinger, D. Y., Goltz, S. M., Davidson, E. A., Lee, J. T., Tu, K., & Valentine, H. T. (1999). Seasonal patterns and environmental control of carbon dioxide and water vapour exchange in an ecotonal boreal forest. *Global Change Biology*, *5*, 891−902.

Houborg, R. M., & Soegaard, H. (2004). Regional simulation of ecosystem CO2 and water vapor exchange for agricultural land using NOAA AVHRR and Terra MODIS satellite data. Application to Zealand, Denmark. *Remote Sensing of Environment*, *93*, 150−167.

Huete, A. (2006). *personal communication.*

Huete, A., Didan, K., Miura, T., Rodriguez, E. P., Gao, X., & Ferreira, L. G. (2002). Overview of the radiometric and biophysical performance of the MODIS vegetation indices. *Remote Sensing of Environment*, *83*, 195−213.

Huete, A. R. (1988). A soil-adjusted vegetation index (SAVI). *Remote Sensing of Environment*, *25*, 295−309.

Impens, I., & Lemur, R. (1969). Extinction of net radiation in different crop canopies. *Theoretical and Applied Climatology*, *17*, 403−412.

Irmak, S., Irmak, A., Jones, J. W., Howell, T. A., Jacobs, J. M., Allen, R. G., et al. (2003). Predicting daily net radiation using minimum climatological data. *Journal of Irrigation and Drainage Engineering*, *129*, 256−269.

Jarvis, P. G., & McNaughton, K. G. (1986). Stomatal control of transpiration: scaling up from leaf to region. *Advances in Ecological Research*, *15*, 1−49.

Jin, M., Dickinson, R. E., & Vogelmann, A. M. (1997). A comparison of CCM2-BATS skin temperature and surface air temperature with satellite and surface observations. *Journal of Climate*, *10*, 1505−1524.

June, T., Evans, J. R., & Farquhar, G. D. (2004). A simple new equation for the reversible temperature dependence of photosynthetic electron transport: A study on soybean leaf. *Functional Plant Biology*, *31*, 275−283.

Jury, W. A., & Tanner, C. B. (1975). Advection modification of the Priestley and Taylor evapotranspiration formula. *Agronomy Journal*, 67.

Kalluri, S. N., & Dubayah, R. O. (1995). Comparison of atmospheric correction models for thermal bands of the Advanced Very High Resolution Radiometer over FIFE. *Journal of Geophysical Research*, *100*, 25411−25418.

Kidwell, K. (1991). NOAA polar orbiter data user's guide. NCDC/SDSD. *National Climatic Data Center.*

Knohl, A., Schulze, E. D., Kolle, O., & Buchmann, N. (2003). Large carbon uptake by an unmanaged 250-year-old deciduous forest in Central Germany. *Agricultural and Forest Meteorology*, *118*, 151−167.

Kustas, W. P., & Daughtry, C. S. T. (1990). Estimation of the soil heat flux/net radiation ratio from spectral data. *Agricultural and Forest Meteorology*, *39*, 205−223.

Kustas, W. P., & Norman, J. M. (1996). Use of remote sensing for evapotranspiration monitoring over land surfaces. *Hydrological Sciences Journal*, *41*, 495−516.

Kustas, W. P., Daughtry, C. S. T., & Vanoevelen, P. J. (1993). Analytical treatment of the relationships between soil heat flux/net radiation ratio and vegetation indices. *Remote Sensing of Environment*, *46*, 319−330.

Lakshmi, V., & Susskind, J. (2000). Comparison of TOVS derived land surface variables with ground observations. *Journal of Geophysical Research*, *105*, 2179−2190.

Lakshmi, V., Small, J., & Goetz, S. (2002). Comparison of surface meteorological variables from TOVS and AVHRR. *Remote Sensing of Environment*, *79*, 176−188.

Lambert, J. (1760). *Photometria Sive de Mensura et Gradibus Luminus, Colorum et Umbrae.* Eberhard Klett.

Lawrence, D. M., & Slingo, J. M. (2004). An annual cycle of vegetation in a GCM. Part I: implementation and impact on evaporation. *Climate Dynamics*, *22*, 87−105.

Leuning, R., Cleugh, H. A., Zegelin, S. J., & Hughes, D. (2005). Carbon and water fluxes over a temperate Eucalyptus forest and a tropical wet/dry savanna in Australia: Measurements and comparison with MODIS remote sensing estimates. *Agricultural and Forest Meteorology*, *129*, 151−173.

Los, S. O., Collatz, G. J., Malmstrom, C. M., Pollack, N. H., DeFries, R. S., Bounoua, L., et al. (2000). A global 9-year biophysical land surface dataset from NOAA AVHRR data. *Journal of Hydrometeorology*, *1*, 183−199.

Madsen, H., Rasmussen, P. F., & Rosbjerg, D. (1997). Comparison of annual maximum series and partial duration series methods for modeling extreme hydrologic events 1. At-site modeling. *Water Resources Research*, *33*, 747−757.

Martin, T. A., Brown, K. J., Cermak, J., Ceulemans, R., Kucera, J., Meinzer, F. C., et al. (1997). Crown conductance and tree and stand transpiration in a second-growth *Abies amabilis* forest. *Canadian Journal of Forest Research*, *27*, 797−808.

Massman, W. J. (1992). A surface-energy balance method for partitioning evapotranspiration data into plant and soil components for a surface with partial canopy cover. *Water Resources Research*, *28*, 1723−1732.

Massman, W. J., & Ham, J. M. (1994). An evaluation of a surface energy balance method for partitioning ET data into plant and soil components for a surface with partial canopy cover. *Agricultural and Forest Meteorology*, *67*, 253−267.

Maurer, E. P., Wood, A. W., Adam, J. C., Lettenmaier, D. P., & Nijssen, B. (2002). A long-term hydrologically based dataset of land surface fluxes and states for the conterminous United States. *Journal of Climate*, *15*, 3237−3251.

McNaughton, K. G., & Black, T. A. (1973). A study of evapotranspiration from a Douglas fir forest using the energy balance approach. *Water Resources Research*, *9*, 1579−1590.

McNaughton, K. G., & Jarvis, P. G. (1991). Effects of spatial scale on stomatal control of transpiration. *Agricultural and Forest Meteorology*, *54*, 279−302.

McNaughton, K. G., & Spriggs, T. W. (1986). A mixed-layer model for regional evaporation. *Boundary-Layer Meteorology*, *34*, 243−262.

Mintz, Y., & Walker, G. K. (1993). Global fields of soil moisture and land surface evapotranspiration dervied from observed precipitation and surface air temperature. *Journal of Applied Meteorology*, *32*, 1305−1334.

Moncrieff, J. B., Massheder, J. M., De Bruin, H. A. R., Elbers, J., Friborg, T., Heusinkveld, B., et al. (1997). A system to measure surface fluxes of momentum, sensible heat, water vapour and carbon dioxide. *Journal of Hydrology*, *189*, 589−611.

Monson, R. K., Turnipseed, A. A., Sparks, J. P., Harley, P. C., Scott-Denton, L. E., Sparks, K., et al. (2002). Carbon sequestration in a high-elevation, subalpine forest. *Global Change Biology*, *8*, 459−478.

Monteith, J. L. (1965). Evaporation and the environment. *Symposium of the Society of Exploratory Biology*, *19*, 205−234.

Morton, F. I. (1983). Operational estimates of areal evapotranspiration and their significance to the science and practice of hydrology. *Journal of Hydrology*, *66*, 1−76.

Motell, C., Porter, J., Foster, J., Bevis, M., & Businger, S. (2002). Comparison of precipitable water over Hawaii using AVHRR-based split-window techniques, GPS and radiosondes. *International Journal of Remote Sensing*, *23*, 2335−2339.

Mukammal, E. I., & Neumann, H. H. (1977). Application of the Priestley–Taylor evaporation model to assess the influence of soil moisture on the evaporation from a large weighing lysimter and class A pan. *Boundary-Layer Meteorology*, *12*, 243−256.

New, M., Hulme, M., & Jones, P. (1999). Representing twentieth-century space-time climate variability. Part I: Development of a 1961–90 mean monthly terrestrial climatology. *Journal of Climate*, *12*, 829−856.

New, M., Hulme, M., & Jones, P. (2000). Representing twentieth-century space-time climate variability. Part II: Development of 1901–1996 monthly grids of terrestrial surface climate. *Journal of Climate*, *13*, 2217−2238.

Nishida, K., Nemani, R. R., Running, S. W., & Glassy, J. M. (2003). An operational remote sensing algorithm of land surface evaporation. *Journal of Geophysical Research-Atmospheres*, *108*, 4270.

Norman, J. M., Kustas, W. P., & Humes, K. S. (1995). Source approach for estimating soil and vegetation energy fluxes in observations of directional radiometric surface-temperature. *Agricultural and Forest Meteorology*, *77*, 263−293.

Ol'dekop, E. M. (1911). On evaporation from the surface of river basins: Trans. Met. Obs. lur-evskogo. *Univ. Tartu*, *Vol. 4*.

Pike, J. G. (1964). The estimation of annual run-off from meteorological data in a tropical climate. *Journal of Hydrology*, *2*, 116−123.

Pinker, R. T., & Laszlo, I. (1992). Modeling surface solar irradiance for satellite applications on a global scale. *Journal of Applied Meteorology*, *31*, 194−211.

Potter, C. S., Randerson, J. T., Field, C. B., Matson, P. A., Vitousek, P. M., Mooney, H. A., et al. (1993). Terrestrial ecosystem production: A process based model based on global satellite and surface data. *Global Biogeochemical Cycles*, *7*, 811−841.

Priestley, C. H. B., & Taylor, R. J. (1972). On the assessment of surface heat flux and evaporation using large scale parameters. *Monthly Weather Review*, *100*, 81−92.

Prince, S. D., Goetz, S. J., Dubayah, R. O., Czajkowski, K. P., & Thawley, M. (1998). Inference of surface and air temperature, atmospheric precipitable water and vapor pressure deficit using AVHRR satellite observations: Validation of algorithms. *Journal of Hydrology*, *212–213*, 230−250.

Ross, J. (1976). Radiative transfer in plant communities. In J. L. Monteith (Ed.), *Vegetation and the atmosphere* (pp. 13−56). London: Academic Press.

Rossow, W. B., Walker, A. W., Beuschel, D. E., & Roiter, M. D. (1996). International Satellite Cloud Climatology Project (ISCCP): Documentation of new cloud data sets. *World Meteorological Organization*, *115*.

Running, S. W., Thornton, P. E., Nemani, R. R., & Glassy, J. M. (2000). Global terrestrial gross and net primary productivity from the Earth Observing System. In O. E. Sala, R. B. Jackson, H. A. Mooney, & R. W. Howarth (Eds.), *Methods in ecosystem science.* New York: Springer-Verlag New York Inc.

Rushdi, A. M., & Kafrawy, K. F. (1988). Uncertainty propagation in fault-tree analyses using an exact method of moments. *Microelectronics Reliability*, *28*, 945−965.

Schmid, H. P., Grimmond, C. S. B., Cropley, F., Offerle, B., & Su, H. B. (2000). Measurements of CO2 and energy fluxes over a mixed hardwood forest in the mid-western United States. *Agricultural and Forest Meteorology*, *103*, 357−374.

Schreiber, P. (1904). Über die Beziehungen zwischen dem Niederschlag und der Wasserführung der Flüße in Mitteleuropa. *Zeitschrift fur Meteorologie*, *21*, 441−452.

Schubert, S., Suarez, M., Park, C. K., & Moorthi, S. (1993). GCM simulations of intraseasonal variability in the Pacific North-American region. *Journal of the Atmospheric Sciences*, *50*, 1991−2007.

Self, S., Rampino, M. R., Zhao, J., & Katz, M. G. (1997). Volcanic aerosol perturbations and strong El Nino events: No general correlation. *Geophysical Research Letters*, *24*, 1247−1250.

Sellers, P. J., Meeson, B. W., Hall, F. G., Asrar, G., Murphy, R. E., Schiffer, R. A., et al. (1995). Remote sensing of the land surface for studies of global change: Models–algorithms–experiments. *Remote Sensing of Environment*, *51*, 3−26.

Shuttleworth, W. J., & Calder, I. R. (1979). Has the Priestley–Taylor equation any relevance to forest evaporation? *Journal of Applied Meteorology*, *18*, 639−646.

Shuttleworth, W. J., & Wallace, J. S. (1985). Evaporation from sparse crops—An energy combination theory. *Quarterly Journal of the Royal Meteorological Society*, *111*, 839−855.

Shuttleworth, W. J., Gash, J. H., Lloyd, C. R., Moore, C. J., Roberts, J., Filho, A. O. M., et al. (1984). Eddy correlation measurements of energy partition for Amazonian forest. *Quarterly Journal of the Royal Meteorological Society*, *110*, 1143−1162.

Sims, D. A., Rahman, A. F., Cordova, V. D., Baldocchi, D. D., Flanagan, L. B., Goldstein, A. H., et al. (2005). Midday values of gross CO2 flux and light use efficiency during satellite overpasses can be used to directly estimate eight-day mean flux. *Agricultural and Forest Meteorology*, *131*, 1−12.

Smith, W. L. (1966). Note on the relationship between total precipitable water and surface dew point. *Journal of Applied Meteorology*, *5*, 726−727.

Sobrino, J. A., & El Kharraz, J. (2003). Surface temperature and water vapour retrieval from MODIS data. *International Journal of Remote Sensing*, *24*, 5161−5182.

Stackhouse, P. W., Gupta, S. K., Cox, S. J., Chiacchio, M., & Mikovitz, J. C. (2000). The WCRP/GEWEX Surface Radiation Budget Project Release 2: An assessment of surface fluxes at 1° resolution. In W. L. Smith, & Y. M. Timofeyev (Eds.), *IRS 2000: Current problems in atmospheric radiation* (pp. 24−29). St. Petersburg, Russia: International Radiation Symposium.

Steven, M. D., Malthus, T. J., Baret, F., Xu, H., & Chopping, M. J. (2003). Intercalibration of vegetation indices from different sensors systems. *Remote Sensing of Environment*, *88*, 412−422.

Stewart, R. B., & Rouse, W. R. (1977). Substantiation of the Priestley and Taylor parameter alpha = 1.26 for potential evaporation in high latitudes. *Journal of Applied Meteorology*, *16*, 649−650.

Stone, P. H., Chow, S., & Quirr, W. J. (1977). July climate and a comparison of January and July climates simulated by GISS general circulation model. *Monthly Weather Review*, *105*, 170−194.

Su, H., Wood, E. F., McCabe, M. F., & Su, Z. (2007). Evaluation of remotely sensed evapotranspiration over the CEOP EOP-1 reference sites. *Journal of the Meteorological Society of Japan*, *85A*, 439−459.

Tateishi, R., & Ahn, C. H. (1996). Mapping evapotranspiration and water balance for global land surfaces. *ISPRS Journal of Photogrammetry and Remote Sensing*, *51*, 209−215.

Thornthwaite, C. W. (1948). An approach toward a rational classification of climate. *Geographical Review*, *38*, 55−94.

Turc, L. (1954). Le bilan d'eau des sols. Relation entre la précipitation, l'évaporation et l'écoulement. *Annales Agronomiques*, *5*, 491−569.

Turner, M. G. (1989). Landscape ecology: The effect of pattern on process. *Annual Review of Ecology and Systematics*, *20*, 171−197.

Vörösmarty, C. J., Federer, C. A., & Schloss, A. L. (1998). Potential evaporation functions compared on US watersheds: Possible implications for global-scale water balance and terrestrial ecosystem modeling. *Journal of Hydrology*, *207*, 147−169.

Warnick, K. F., & Chew, W. C. (2004). Error analysis of the moment method. *IEEE Antennas and Propagation Magazine*, *46*, 38−53.

Willmott, C. J. (1982). Some comments on the evaluation of model performance. *Bulletin of the American Meteorological Society*, *11*, 1309−1313.

Wilson, K., Goldstein, A., Falge, E., Aubinet, M., Baldocchi, D., Berbigier, P., et al. (2002). Energy balance closure at FLUXNET sites. *Agricultural and Forest Meteorology*, *113*, 223−243.

Wofsy, S. C., Goulden, M. L., Munger, J. W., Fan, S. M., Bakwin, P. S., Daube, B. C., et al. (1993). Net exchange of CO2 in a mid-latitude forest. *Science*, *260*, 1314−1317.

Xiao, X., Hollinger, D., Aber, J. D., Goltz, M., Davidson, E., Zhang, Q., et al. (2003). Satellite-based modeling of gross primary production in an evergreen needleleaf forest. *Remote Sensing of Environment*, *89*, 519−534.

Xu, L. K., & Baldocchi, D. D. (2004). Seasonal variation in carbon dioxide exchange over a Mediterranean annual grassland in California. *Agricultural and Forest Meteorology*, *123*, 79−96.

Zhang, Q., Xiao, X., Braswell, B. H., Linder, E., Aber, J., & Moore, B. (2005). Estimating seasonal dynamics of biophysical and biochemical parameters in a deciduous forest using MODIS data and a radiative transfer model. *Remote Sensing of Environment*, *99*, 357−371.